



UNSW
SYDNEY

School of Mechanical and Manufacturing Engineering

Faculty of Engineering

The University of New South Wales

Development of an Open-Source CubeSat Reaction Wheel System

by

Mark Yeo

Thesis submitted as a requirement for the degree of
Bachelor of Engineering in Mechatronic Engineering

Submitted: 28th May 2018

Student ID: z3461219

Supervisor: A/Prof. Jay Katupitiya

Topic ID: -

Abstract

A commercial reaction wheel system (RWS) for a CubeSat typically costs upwards of \$20 000, making them inaccessible for many CubeSat developers with smaller budgets, which highlights the need for a cheaper alternative. This thesis seeks to meet this need by designing, building and testing an open-source CubeSat RWS. This new design has a parts-cost of under \$1000, and will be kept open-source to allow other developers to further modify, verify and utilise the design. Testing of the built prototype has indicated performance comparable to existing commercial products, showing potential for the design to be further developed into a reliable alternative to commercial RWSs at a significantly reduced cost.

All code and design files for this RWS can be found online at <https://bitbucket.org/bluesat/cubesat-adcs>.

Acknowledgements

I'd like to thank BLUEsat and its past and present members for rekindling my love for space (and for paying for this project), as well as the UNSW Engineering Faculty for funding BLUEsat for all of these years. I'd also like to acknowledge my supervisor A/Prof. Jay Katupitiya for being really chill all the time even though I never came to half of the group meetings.

Eph 2:1-10

Abbreviations

ADCS Attitude Determination and Control System

COTS Commercial Off-The-Shelf

I2C Inter-Integrated Circuit

MCU MicroController Unit

MOI Moment Of Inertia

OBC On-Board Computer

PCB Printed Circuit Board

PWM Pulse-Width Modulation

RF Radio-Frequency

RWS Reaction Wheel System

SPI Serial Peripheral Interface

μ SD MicroSD

Contents

1	Introduction	1
1.1	Problem Statement	2
1.2	Thesis Structure	2
2	Background Context and Literature Review	3
2.1	Background Context	3
2.1.1	CubeSats	3
2.1.2	Attitude Determination and Control Systems	6
2.2	Reaction Wheels	7
2.2.1	Basic Theory and Overview	7
2.2.2	Existing Commercial Off-the-Shelf Components	8
2.2.3	Open-Source Hardware	11
2.3	Reaction Wheel System Design Parameters	13
2.3.1	Wheel Arrangement	14
2.3.2	External Torques	16
2.3.3	Distribution Algorithms	16
2.4	Summary	19
3	Design Overview	20
3.1	Mechanical Design	20

3.1.1	Design Decisions	20
3.1.2	Component Overview	22
3.2	Electrical Design	25
3.2.1	Overview	25
3.3	Hardware Cost Breakdown	29
3.4	Microprocessor Software	30
3.4.1	Controller Task	30
3.4.2	Wheel Distribution	31
3.5	Supporting Hardware	32
4	Performance Testing and Results	35
4.1	Detumbling Performance	35
4.2	Pointing Performance	39
4.3	Momentum Storage Capacity	41
4.4	Power Draw	44
5	Comparison of RWS with Existing Designs	45
5.1	Comparison of Specifications	45
5.2	Comparison of Design Features	46
5.2.1	Prototype Advantages	47
5.3	Prototype Disadvantages	47
5.4	Summary	48
6	Conclusions and Future Work	49
	Bibliography	51
	Appendix RWS Mechanical Drawings	54

Appendix RWS Electrical Schematics	62
Appendix Support Hardware Electrical Schematics	65
Appendix Complete Test Results	68
Appendix Other Datasheets	78

List of Figures

2.1	UNSW's EC0 Satellite - a 2.5U CubeSat. Reproduced from [1]	4
2.2	Istanbul Technical University's CubeSat ITUpSat-1. Reproduced from [2]	5
2.3	Rotational Axes of a Satellite. Reproduced from [3]	6
2.4	COTS CubeSat RWSs. From left to right: Clyde Space's ADCS-TM, GOMspace's NanoTorque GSW-600, NanoAvionic's SatBus 4RW0. Reproduced from [4][5][6]	10
2.5	Photo (left) and Exploded View (right) of Portland State University's Oresat RWS. Reproduced from [7]	13
2.6	Four-Wheel Pyramid Configuration. Reproduced from [8]	14
2.7	Wheel Tilt (β). Reproduced from [9]	15
2.8	Momentum Spaces of an RWS. Physically achievable points are shown in red, while those achievable with the pseudoinverse method are shown in blue. Reproduced from [10].	18
3.1	Maxon EC20 Flat 351005 and Faulhaber 2610B-SC Motors. Reproduced from [11] and [12].	22
3.2	Render of the Assembled RWS	23
3.3	Render of Aluminium Wheel	23
3.4	Photos of Motor Mount without Wheel (left) and with Wheel attached (right).	24
3.5	Photo of Assembled RWS	24
3.6	Block Diagram of RWS Electronics	26
3.7	Schematic of Arduino Connectivity	26

3.8	Schematic of PWM Amplification and Smoothing Circuit	27
3.9	PWM Circuit Input and Output Signals	27
3.10	Photo of Motor Circuit	28
3.11	Schematic of Frequency to Voltage Circuit	29
3.12	Simulation Running Pointing Algorithm (0-90°)	31
3.13	Block Diagram of Satellite Electronics	33
3.14	Photo of Assembled Satellite	34
4.1	Air Bearing Setup for Z-Axis Testing	36
4.2	Detumble Performance around Z+ Axis	36
4.3	Detumble Performance around Z- Axis	37
4.4	Air Bearing Setup for X+Y+ Axis Testing	38
4.5	Detumble Performance around X+Y+ Axis	38
4.6	Detumble Performance around X-Y- Axis	39
4.7	Pointing Performance around Z Axis. Note that the target angle of +180° is shown as -180° for ease of reading.	40
4.8	Pointing Performance around Z Axis (Extended)	40
4.9	Air Bearing Natural Spin Decay. Note that spin was manually reversed at 100s	41
4.10	Setup for Stairwell Suspension Test	42
4.11	Momentum Capacity around Z Axis	43
4.12	Effect of Restoring Torque on Satellite ω	43
4.13	Motor Power Draw from Zero to Full Speed with Maximum Acceleration	44
D.1	Air Bearing Natural Spin Decay. Note that spin was manually reversed at 100s	68
D.2	Detumble Performance around X+ Axis	69
D.3	Detumble Performance around X- Axis	69

D.4 Detumble Performance around Y+ Axis	70
D.5 Detumble Performance around Y- Axis	70
D.6 Detumble Performance around Z+ Axis	71
D.7 Detumble Performance around Z- Axis	71
D.8 Detumble Performance around X+Y+ Axis	72
D.9 Detumble Performance around X-Y- Axis	72
D.10 Pointing Performance around X Axis	73
D.11 Pointing Performance around Y Axis	73
D.12 Pointing Performance around Z Axis. Note that the target angle of +180°is shown as -180°for ease of reading.	74
D.13 Pointing Performance around Z Axis	74
D.14 Momentum Capacity around Y Axis	75
D.15 Momentum Capacity around Z Axis	75
D.16 Momentum Capacity around XY Axis	76
D.17 Motor Power Draw at Zero Speed	76
D.18 Motor Power Draw at Minimum Linear Speed	76
D.19 Motor Power Draw at Full Speed	76
D.20 Motor Power Draw at Medium Speed	77
D.21 Motor Power Draw from Zero to Full Speed with Maximum Acceleration	77

List of Tables

2.1	COTS CubeSat Reaction Wheel Spec Overview. Entries in bold are designed specifically for use in CubeSats. Entries in <i>italics</i> are considered outliers with respect to torque and momentum storage (Max p)	9
2.2	General Range of COTS CubeSat Reaction Wheel Specs	9
2.3	COTS CubeSat RWS Specification Overview. Note that the MAI-400 contains an additional ADCS computer, gyro and magnetometer.	10
3.1	Cost Breakdown of RWS Hardware	29
4.1	RWS Power Draws	44
5.1	Comparison of Specifications of COTS and Prototype Reaction Wheels .	46
5.2	Comparison of Specifications of COTS and Prototype Reaction Wheels (where available). Sources: [4][13][5][6][14]	46

Chapter 1

Introduction

The majority of satellites have a payload or system that requires a particular attitude (orientation) or spin in order to operate correctly. For example, onboard cameras, directional antennas and even some omni-directional antennas have specific requirements on the satellite's attitude and spin. These requirements are handled by the Attitude Determination and Control System (ADCS), responsible for calculating the satellite's current attitude and for controlling the satellite to achieve the required attitude and spin.

The use of a reaction wheel system (RWS) is a common method of actuation used by the ADCS. By varying the speed of weighted disks in the x, y and z-axes, attitude control is achieved by result of the conservation of angular momentum. However, like most space-related hardware, commercially available RWSs are very expensive. This is due to many factors, such as the low demand volume, lack of economy of scale, the high cost of testing and the even higher cost of obtaining space heritage. These costs ultimately are passed down to the buyer, reflected in high purchase prices upwards of AUD\$20,000 for a CubeSat RWS. This affects teams with smaller budgets such as university groups, who develop CubeSats but often settle for cheaper alternatives such as magnetorquers or permanent magnets as a means of achieving attitude control.

This thesis explores a potential solution to this problem by developing an open-source

reaction wheel system (RWS) for a CubeSat. Making the project open-source allows design, testing and verification costs to be spread over several groups, ultimately resulting in a fully-functional, verified design available to the public at the cost of parts and manufacturing only.

1.1 Problem Statement

This thesis aims to design, build and test a functional 3-axis RWS prototype. The design will be made open-source, allowing other CubeSat teams to build on and verify the design, and to ultimately be able to utilise the design for a substantially lower cost than COTS alternatives.

The RWS will need to be capable of detumbling (reducing spin to zero) and orientating itself toward a specified angle on command. Detumble and point functionality will be executed utilising a set of reaction wheels and will require each motor to operate within its speed and torque saturation limits.

1.2 Thesis Structure

This thesis is divided into five main chapters. Chapter 2 covers the background theory behind reaction wheels, a review of existing RWS designs, and literature relevant to reaction wheels. Chapter 3 explains the design of the new design, with justification of the major design decisions made. Chapter 4 outlines the results obtained during testing of the built prototype, with analysis of results to obtain performance metrics. Chapter 5 compares the new design to existing commercial products in terms of performance and specifications. Finally, concluding remarks and suggestions for future work are given in Chapter 6.

Chapter 2

Background Context and Literature Review

This chapter gives a background into CubeSats and attitude control and surveys existing RWSs. Additionally, research has been carried out into both commercial designs and relevant literature to inform design decisions made when designing the open-source RWS.

2.1 Background Context

2.1.1 CubeSats

CubeSats are a class of picosatellites which conform to an open-source standard developed by Cal Poly[15]. Each CubeSat unit is a 10cm cube with a mass of up to 1.33kg, with complete satellites being composed of up to 3 of these units (Figure 2.1 shows a 2.5U satellite). The CubeSat standard specifies various mechanical, electrical and operational requirements, as well as defining the deployment mechanism for interfacing with the launch vehicle.

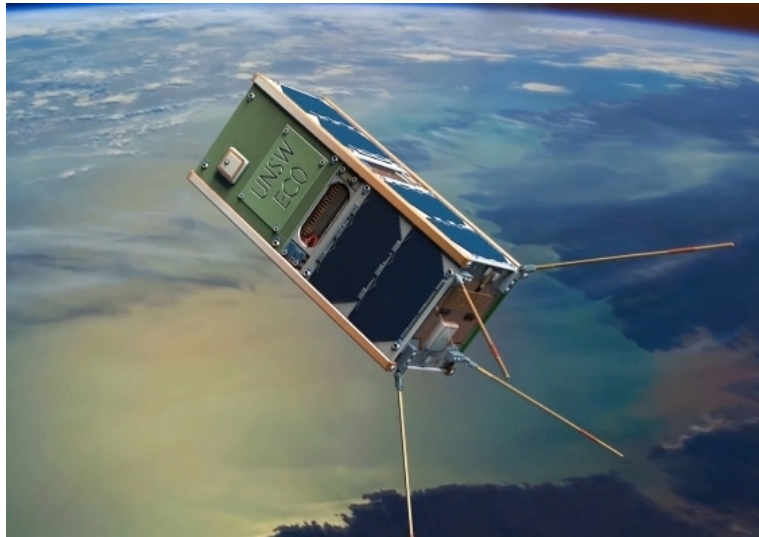


Figure 2.1: UNSW’s EC0 Satellite - a 2.5U CubeSat. Reproduced from [1]

Due to their small size and economy of scale through a standardised design, CubeSats can be launched at a substantially lower cost than traditional micro-satellites [16]. Furthermore, their standardised design allows for a heavy use of commercial off-the-shelf (COTS) components, decreasing overall development time and required technical knowledge [17]. For these reasons, CubeSats provide a low-cost platform for testing small payloads and obtaining space heritage for hardware, making them popular with many academic and hobbyist groups [18].

To date, more than 700 CubeSats have been launched, typically with a mission related to communications, scientific experiments or technology demonstrations [19]. Unsurprisingly, most of these CubeSats are developed by universities - teams focused on once-off experiments or space testing of hardware with typically smaller budgets than commercial and military satellite developers [20]. The majority of CubeSats are launched into Low Earth Orbit, at altitudes between 160km to 2000km [21].

Although there is no formal standard for CubeSat internal electronics, a de facto standard has emerged, based on the PC/104 standard for embedded electronics. This ‘CubeSat PC/104’ standard implements the physical design of the original PC/104 standard (such as the positioning of mounting holes) but uses a different data bus location and pin allocations [22]. The CubeSat PC/104 standard allows printed circuit

boards (PCBs) to be stacked on top of each other, as shown in Figure 2.2.

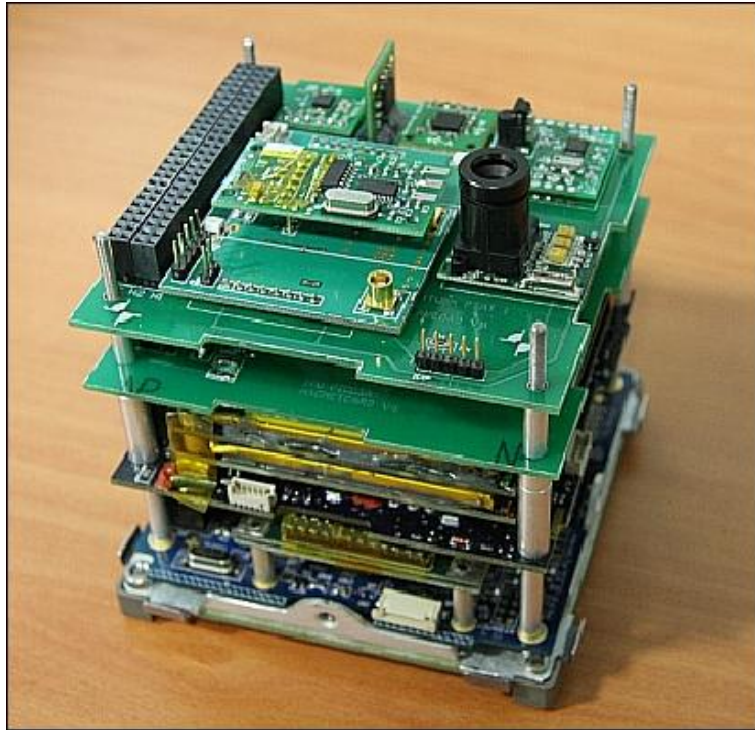


Figure 2.2: Istanbul Technical University's CubeSat ITUpSat-1. Reproduced from [2]

2.1.2 Attitude Determination and Control Systems

The ADCS is a system within the satellite bus that is responsible for both calculating and controlling a satellite's current attitude (orientation) with reference to an inertial reference frame such as the Earth. An ADCS is required on any satellite containing systems with non-trivial attitude requirements. Attitude requirements vary depending on the payload - for example, equipment such as cameras and telescopes require full 3-axis pointing, whereas more omnidirectional equipment such as turnstile antennas simply require the satellite's spin to be below a certain threshold. Figure 2.3 defines the three rotational axes of a generic satellite.

ADCS operations can be split into solving two major tasks - attitude determination and attitude control. Attitude determination involves gathering data from sensors such as gyroscopes, magnetometers and star trackers, followed by data fusion (such as the EKF

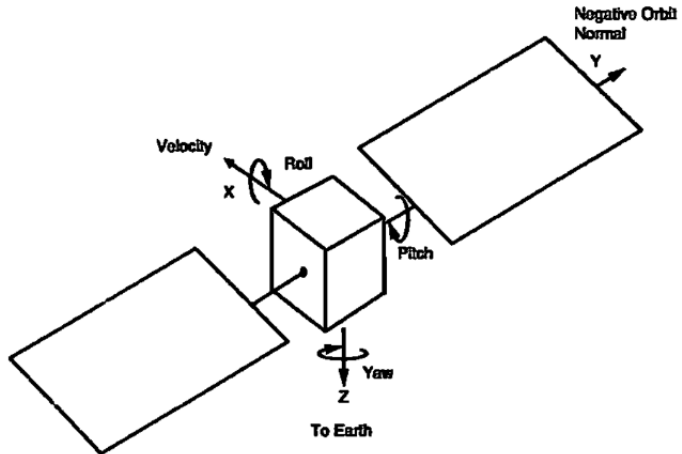


Figure 2.3: Rotational Axes of a Satellite. Reproduced from [3]

and UKF) to calculate the satellite’s attitude. As attitude determination is outside the scope of this thesis, the topic will not be explored further. Attitude control on the other hand involves orienting the satellite to a desired orientation or angular velocity. There are a wide variety of ADCS actuators available for use, including hysteresis rods, magnetorquers (electromagnets), thrusters, gravity booms, reaction wheels and control moment gyroscopes. Each method has its own strengths and weaknesses, and as such, a combination of actuators is typically chosen to suit the attitude requirements of the mission. Non-reaction-wheel actuation methods also fall outside the scope of this thesis - as such they have not been covered in depth here. Additional information on other attitude control methods can be found in Wertz’s *Space Mission Analysis and Design*[3].

2.2 Reaction Wheels

This section covers the theory behind reaction wheels and their use in attitude control.

2.2.1 Basic Theory and Overview

A reaction wheel is a flywheel used for attitude control in a satellite. Through the conservation of angular momentum, any change to the speed of rotation of a wheel causes the satellite's orientation to counter-rotate along the axis parallel to the wheel's axis of rotation. Furthermore, as a result of Newton's 3rd law, the torque imparted on the satellite by the acceleration of the wheel is equal and opposite to torque imparted on the wheel by the satellite. Mathematically, this is given by:

$$\begin{aligned} I_{satellite}\dot{\theta}_{satellite} + I_{wheel}\dot{\theta}_{wheel} &= L_{total} \\ I_{satellite}\ddot{\theta}_{satellite} + I_{wheel}\ddot{\theta}_{wheel} &= 0 \end{aligned}$$

when external torques are ignored, and L_{total} is a constant. Full three-axis control can then be achieved with three wheels whose axes are not parallel and do not lie along the same plane - this is typically done with one wheel oriented along each axis of the satellite (x,y,z).

Reaction wheels provide several advantages over other forms of ADCS actuation. Firstly, they provide fast attitude control, allowing target orientations to be reached in a matter of seconds to minutes [23] as opposed to some actuation methods (such as magnetorquers) that take several hours to days to correctly orient a satellite. Secondly, they require only electricity to function, whereas other actuation methods expend non-renewable resources (e.g. thrusters) or are dependent on external fields (e.g. magnetorquers and gravity gradient booms). Thirdly, by utilising multiple reaction wheels, full 3-axis control can be achieved - whereas some other actuation methods only provide 2-axis control (e.g. magnetorquers and gravity booms).

However, reaction wheels also have several disadvantages. Firstly, reaction wheels involve moving components, which increases the probability of failure over the satellite's lifetime compared to static actuators (e.g. magnetorquers). Secondly, the mass, volume and arrangement volume of each reaction wheel dictates that a large proportion of the satellite's mass and volume budgets are taken up by an RWS (roughly half of a 1U's mass and volume budget - see Table 2.3 in Section 2.2.2). Thirdly, if a satellite requires

its current orientation and angular velocity to be preserved, the speed of the reaction wheels must be held constant, resulting in a large power draw if a non-zero angular velocity is required. Finally, changes in flywheel speed accumulate over time, which results in the possibility of motor speed saturation. When this happens, it is necessary to de-spin wheels, or ‘momentum dump’ through the use of any actuator that can change a satellite’s total angular momentum (e.g. thrusters, magnetorquers, etc.).

2.2.2 Existing Commercial Off-the-Shelf Components

This section gives a survey of the majority of COTS reaction wheel products available in 2018. The two categories of products considered are single reaction wheels and complete reaction wheel systems.

Individual Reaction Wheels

Reaction wheels are usually sold as individual units, with integrated motor driving circuitry allowing each wheel to be controlled via serial communication. Wheels typically provide mounting points for positioning in various configurations. Table 2.1 gives an overview of COTS CubeSat reaction wheel specifications.

From Table 2.1, we discard outliers with respect to torque and momentum storage (i.e. CubeWheel S, RWP100, RW1 and RW35). From the remaining wheels we see a specification range given in Table 2.2.

Reaction Wheel Systems

Reaction wheels are sometimes sold as complete RWSs including three or four reaction wheels to provide full three-axis attitude control. Wheels are controlled over serial

Table 2.1: COTS CubeSat Reaction Wheel Spec Overview.

Entries in **bold** are designed specifically for use in CubeSats. Entries in *italics* are considered outliers with respect to torque and momentum storage (Max p)

Company	RW Name	Torque (mNm)	Max p (mNms)	Max Speed (rpm)	Ave Power (W)	Mass (g)	Price (USD)	Source
MAI Aero	MAI-400 RW	0.635	11	10000	0.85	110	7100	[24]
Gomspace	GSW-600	2	19	6000	0.35	180	-	[5]
NanoAvionics	Single RW	3.2	22	6500	0.15	155	-	[6]
CubeSpace	CubeWheel L	2.3	30	6000	0.27	220	7685	[25]
CubeSpace	CubeWheel M	1	10	6000	0.24	140	6385	[25]
CubeSpace	<i>CubeWheel S</i>	0.23	1.7	8000	0.12	60	5085	[25]
Blue Canyon Tech (BCT)	RWP015	4	15	-	0.6	130	-	[26]
BCT	RWP050	7	50	-	0.5	240	-	[27]
BCT	<i>RWP100</i>	7	100	-	0.5	350	-	[28]
Astrofein	<i>RW1</i>	0.023	0.58	16000	0.62	20	-	[29]
Astrofein	<i>RW35</i>	5	100	5000	4.5	500	-	[29]

Table 2.2: General Range of COTS CubeSat Reaction Wheel Specs

Specification	Value
Torque (mNm)	0.635 - 7
Max Momentum (mNms)	10 - 50
Max Speed (rpm)	6000 - 10000
Ave Power (W)	0.15 - 0.85
Mass (g)	110 - 250
Price (USD)	6385 - 7685

communication either directly to the wheels or via an on-board processor. Table 2.3 gives an overview of existing COTS RWSs, with a selection shown in Figure 2.4.

Table 2.3: COTS CubeSat RWS Specification Overview.
Note that the MAI-400 contains an additional ADCS computer, gyro and magnetometer.

Company	RWS Name	Arrangement	Mass (g)	Dimensions (mm)	Price (USD)	Source
Clyde Space	ADCS-TM	3-wheel xyz	236	70 x 70 x 35	-	[4]
MAI Aero	MAI-400	3-wheel xyz	694	100 x 100 x 51.6	34,420	[13]
Gomspace	NanoTorque GSW-600	4-wheel pyramid	940	95 x 95 x 61.6	-	[5]
NanoAvionics	SatBus 4RW0	4-wheel pyramid	720	92.5x92.5x51.3	17,715	[6]
Blue Canyon Tech	Flexcore	4-wheel pyramid	850	100 x 100 x 50	-	[14]

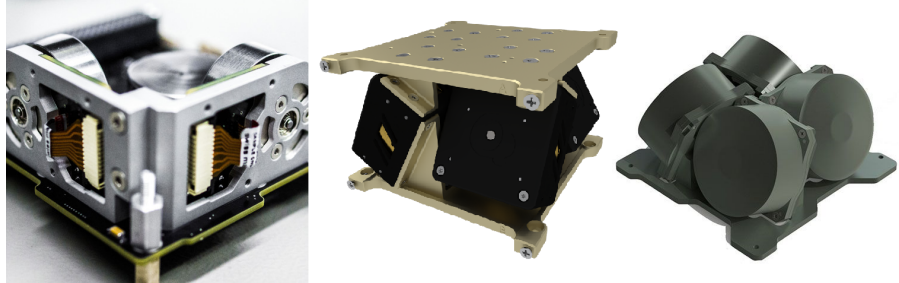


Figure 2.4: COTS CubeSat RWSs.

From left to right: Clyde Space’s ADCS-TM, GOMspace’s NanoTorque GSW-600, NanoAvionic’s SatBus 4RW0. Reproduced from [4][5][6]

From this table we can see that most COTS RWSs take up roughly half of the volume and mass budgets of a 1U. Interestingly, the RWSs with pyramid arrangements do not have include CubeSat connecting headers.

Cost Viability for CubeSat Missions

A fully functional 1U CubeSat (without a RWS) can be built for as low as \$50,000 [30], with launch costs upwards of around a similar price [31]. This low cost is one of the many advantages of CubeSats, providing a pathway for students, small businesses and highly experimental payloads to gain access to space. However, it is clear from Tables 2.2 and 2.3 that the cost of a reaction wheel system (with three or four wheels) is generally upwards of USD\$20,000, which would increase the cost of a cheap CubeSat by almost 50%. This may be an acceptable cost to larger businesses and research groups, but for many the high price places a commercial RWS out of reach. Groups with limited budgets thus often opt for cheaper actuation methods (e.g. magnetorquers) [32] or design their own reaction wheels in-house [23][33][34], which usually comes at the cost of decreased attitude control and increased risk of component failure for each option respectively.

However, this high cost for commercial reaction wheels is not unjustified, due to the wide range of factors contributing to the total cost. Among these factors include the cost of parts and labour, extensive testing to guarantee performance in space, costs to

obtain flight heritage, as well as business overhead and profit margin. These factors, combined with the very low demand for CubeSat components (compared to almost any other publicly sold product), all contribute to high costs which are passed onto the end-user (i.e. satellite developers). Even if components are developed in-house, budget and development time restrictions may limit the quality and reliability of the final product. Thus, an alternative method of development is needed.

2.2.3 Open-Source Hardware

Open-source hardware (OSH) refers to physical products which are developed collaboratively, where both hardware and software design information is publicly shared for anyone to use, develop and modify. OSH allows multiple developers and groups to work on and test a design, effectively distributing the costs over many different groups. In addition to this, OSH also shares benefits by allowing users to use and modify the design for free. This allows developers to reuse code and hardware designs, reducing overall development times and costs [35].

When compared to closed-source products (the majority of COTS products), there are several benefits of OSH to the end-user aside from cost. These include the ability to bypass vendor lock-in caused by incompatibility of products across vendors, ability to completely customise the design to meet requirements, and with time, and a higher reliability due to a greater pool of peer-reviewing of the design and code [36]. However, OSH also has several disadvantages, such as having a longer development time if few developers uptake the project, and requiring a higher level of technical knowledge to customise designs.

There have been several examples of successful OSH products, including but not limited to: the Arduino microcontroller range, Sparkfun and Adafruit electronics, the RepRap 3D printer project and the Lasersaur laser cutter.

Existing Open-Source Hardware RWSs

Although there are many papers detailing the design of ADCSs for particular CubeSat missions [23][33][37], these papers are usually directed towards the theory-side of ADCSs and contain only a high-level systems view of their designs. As of 2018, only one open-source RWS design currently exists, outlined below.

Portland State University’s OreSat RWS In 2016, Portland State University developed an open-source RWS for a 2U CubeSat [7], shown in Figure 2.5. The RWS features 4 reaction wheels in a pyramid configuration, with an inbuilt 9-DoF IMU providing basic orientation data. It was designed for rapid prototyping and was built over the course of 8 weeks, relying on 3D printed structures and several COTS components to allow for rapid design iteration cycles. The built design was tested successfully in a drop tower, demonstrating detumbling around its vertical axis. However, to facilitate ground testing, the design utilised motors with substantially more torque and speed than would be required for a CubeSat in orbit, with the developers noting that a flight version would use more appropriate motors. Unfortunately, developing upon the existing design would likely be problematic as a change in motors and wheel shapes would trigger major design changes in both the inwards-facing pyramid motor arrangement and the supporting electronics.

Based on this discussion, it is proposed that a new open-source RWS be developed with parameters suited for operation in space.

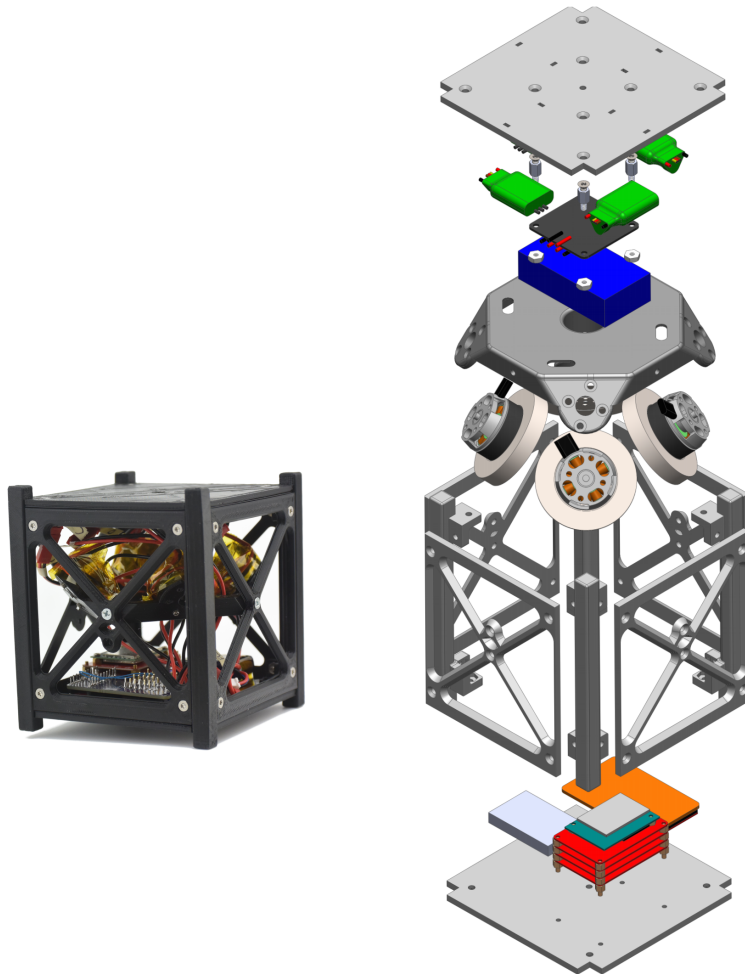


Figure 2.5: Photo (left) and Exploded View (right) of Portland State University's Oresat RWS. Reproduced from [7]

2.3 Reaction Wheel System Design Parameters

This section seeks to characterise the typical design parameters and specifications used in a RWS. In addition to the existing commercial designs (previously summarised in Table 2.2 and 2.3), this data will be used to inform design decisions when designing the RWS (in Section 3).

2.3.1 Wheel Arrangement

Full three-axis control is typically achieved with three wheels oriented along each axis (x,y,z) of the satellite, previously shown in Figure 2.4. Additionally, any configuration of three wheel orientations is valid as long as each wheel axis is not parallel or on the same plane as the other two wheel axes. As such, satellites are often equipped with four wheels with every combination of three wheels satisfying the aforementioned condition [8]. This provides both redundancy in case a motor fails, and also provides better torque and momentum storage. A popular four-wheel configuration is the pyramid configuration where identical wheels are placed pointing outwards on each side of a square pyramid, as shown in Figure 2.6. Note that the direction of wheel axes are independent from the positioning of the wheels themselves - as such, RWSs with a pyramid configuration typically shift the wheel positions to maximise the size of the wheels while minimising the envelope volume (previously seen in 2.4).

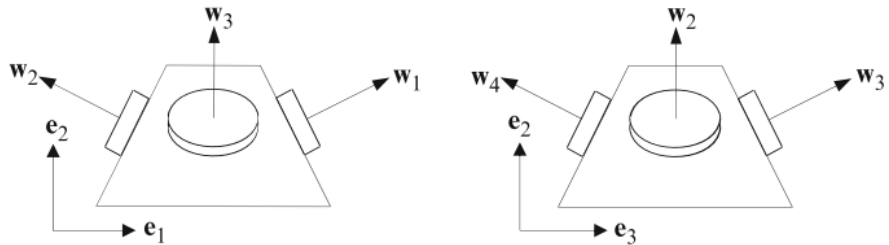


Figure 2.6: Four-Wheel Pyramid Configuration. Reproduced from [8]

Tilt Angle (Pyramid Configuration)

The main parameter in the pyramid configuration is the angle of tilt of the wheels. This is usually measured by the angle of elevation of the wheel axes (β) as shown in Figure 2.7. The momentum space of pyramid-configuration reaction wheels (the maximum momentum capacity of the RWS in any given direction) is maximised when $\beta = \sin^{-1} \left(\frac{1}{\sqrt{3}} \right) \text{ rad} = 35.26^\circ$ [38][10]. This value of β is appropriate for satellites with fairly similar moments of inertia along their x , y and z axes, e.g. 1U CubeSats.

For larger CubeSats (e.g. 2U, 3U) a smaller value for β must be used. A study by

Shirazi and Mirshams [9] simulated a satellite with moment of inertias (MOIs) of [6, 12, 13]kg.m² to find the optimum tilt angle. It was found that minimal power consumption was achieved with a tilt angle of 32°.

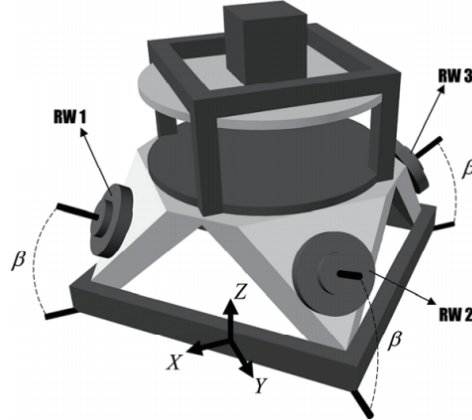


Figure 2.7: Wheel Tilt (β). Reproduced from [9]

To apply this result to CubeSats, we firstly observe that the MOIs in the study correspond to a ratio of 1 : 2 : 2.17. Given that a cuboid of uniform mass has a MOI of $I_h = m/12 * (w^2 + d^2)$, we then substitute in the dimensions for 1U-3U CubeSats [15]. From this it can easily be found that 1.5U and 2U CubeSats give MOI ratios of 1 : 1.625 : 1.625 and 1 : 2.5 : 2.5 respectively. Additionally, it can be seen that the optimal tilt angle must decrease as a CubeSat's MOI ratio becomes more unbalanced (for longer, higher-U CubeSats) as more of each wheel axis component must be in the x and y directions. Thus, we can apply this study's result to CubeSats, concluding that the optimum minimum-power tilt angle for CubeSats of 2U or greater should generally be below 32°, assuming a uniform mass distribution. Conversely, the optimum minimum-power tilt angle for 1U CubeSats should be above 32 °. These results are in accordance with the previous paragraph's β analysis, as well as the survey of 4-wheel CubeSat COTS products, which are designed for 2U+ CubeSats and have a β of around 30°[5][6][14]. Thus, a RWS should have a β of around 30°- 35°depending on the size of the CubeSat it is designed for.

2.3.2 External Torques

To operate effectively, an RWS must have the capacity to counteract external torques acting on the satellite. These torques can be categorised into cyclical and secular torques [3].

Cyclical torques vary in a sinusoidal manner and average out over an orbit, including solar radiation (for earth-oriented satellites) and interaction with the Earth's magnetic field. Cyclical torques may be absorbed and then released by reaction wheels with sufficient momentum storage.

Secular torques accumulate over time and do not average out over an orbit, including aerodynamic drag (for earth-oriented satellites) and solar radiation (for solar-oriented satellites). Secular torques are not dependent on orbital position and do not average out to zero, causing reaction wheels to saturate over time. The effects of these secular torques can be temporarily stored within a RWS but must ultimately be dissipated with an different attitude control method.

A study by Oland and Schlanbusch [39] found that for a CubeSat, solar radiation imparted a torque of roughly 1.5×10^{-8} Nm, internal magnetic fields produced a disturbance torque of up to 1×10^{-6} Nm, and atmospheric drag was roughly 1.2×10^{-7} Nm for altitudes above 700km. A different study by Li et al. [32] found that for a CubeSat in a circular orbit at an altitude of 500km, total disturbance torques (both secular and cyclical) are estimated to be roughly 5×10^{-7} Nm, roughly of the same order of magnitude as the sum of values found in the former study. Thus, a RWS should be able to exert a torque of at least 1×10^{-6} Nm along any axis.

2.3.3 Distribution Algorithms

Once the total torque or angular momentum for the RWS is decided, it must then be transformed from the body frame into the wheel frame. That is, individual wheels must be run at the correct speeds such that the sum of wheel torques or angular

momentums generated by the RWS is equal to the desired total sum. The problem is given mathematically below, from [8]:

Let \mathbf{W}_n be a $3 \times n$ distribution matrix where the columns are unit vectors parallel to the spin axes of the n wheels. Then,

$$\mathbf{W}_n = [\mathbf{w}_1 \mathbf{w}_2 \dots \mathbf{w}_n]$$

Let the total wheel torque and angular momentum in the body frame be given as \mathbf{L}_B and \mathbf{H}_B respectively. Then,

$$\begin{aligned}\mathbf{L}_B &= \mathbf{W}_n [L_1 L_2 \dots L_B]^T \equiv \mathbf{W}_n \mathbf{L}_W \\ \mathbf{H}_B &= \mathbf{W}_n [H_1 H_2 \dots H_B]^T \equiv \mathbf{W}_n \mathbf{H}_W\end{aligned}$$

where \mathbf{L}_W and \mathbf{H}_W are vectors containing each individual wheels' torque and angular momentum. The problem then becomes: for a given \mathbf{L}_B , \mathbf{H}_B and \mathbf{W}_n , find \mathbf{L}_W and \mathbf{H}_W . Since the methods for solving wheel torque and angular momentum are identical, the following discussion will involve angular momentum only.

For the case where there are three wheels aligned in the x, y and z axes,

$$\mathbf{W}_n = \begin{bmatrix} 1 & 0 & 0 \\ 0 & 1 & 0 \\ 0 & 0 & 1 \end{bmatrix}$$

Then there is a single solution where $\mathbf{H}_W = \mathbf{W}_n^{-1} \mathbf{H}_B$.

In the case where there are four wheels in a pyramidal configuration,

$$\mathbf{W}_n = \begin{bmatrix} 0 & -\cos(\beta) & 0 & \cos(\beta) \\ \cos(\beta) & 0 & -\cos(\beta) & 0 \\ \sin(\beta) & \sin(\beta) & \sin(\beta) & \sin(\beta) \end{bmatrix}$$

In this case the system is overactuated, and as such there is no unique way of distributing angular momentum. Two common methods of solving this problem are outlined below.

Pseudoinverse Distribution Law The pseudoinverse of matrix \mathbf{W}_n is given by $\mathbf{W}_n^+ = \mathbf{W}_n^T(\mathbf{W}_n\mathbf{W}_n^T)^{-1}$ which gives a distribution of $\mathbf{H}_W = \mathbf{W}_n^+\mathbf{H}_B$. This is a least squares distribution which minimises the sum of squares of each wheel's angular momentum and overall power draw. Additionally, it is very simple to implement and is not computationally taxing. However, it tends to have a slower performance in attitude control than other methods [8] due to the fact that it cannot utilise 100% of the RWS's momentum space [10] (shown in Figure 2.8).

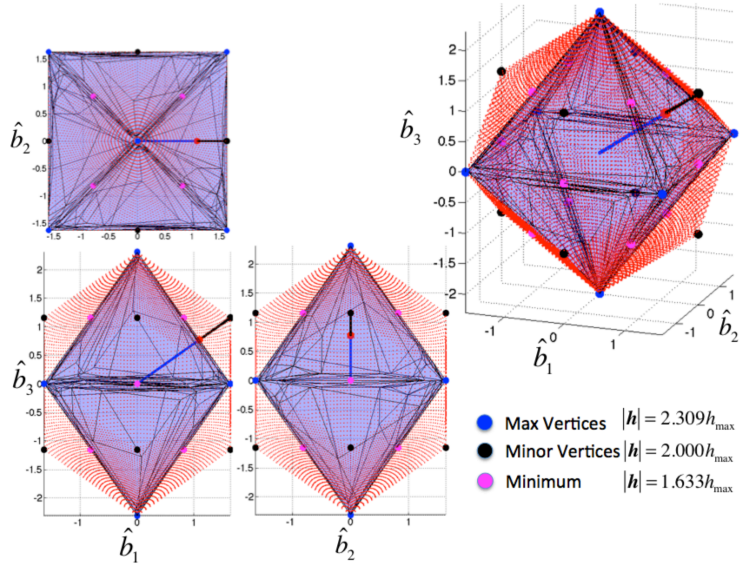


Figure 2.8: Momentum Spaces of an RWS.

Physically achievable points are shown in red, while those achievable with the pseudoinverse method are shown in blue. Reproduced from [10].

Minimax Distribution Law The minimax method distributes angular momentum by minimising the largest angular momentum of the four wheels. This allows for a larger torque and angular momentum capacity than the pseudoinverse method, but can lead to higher and sometimes discontinuous wheel torques in certain conditions. Additionally, this method may result in jitter when wheels are near zero speed or resonant frequencies of the satellite [8].

There are many other methods that can be used for distributing angular momentum, but as this thesis is mainly focused on the development and testing of hardware, these

other methods will not be covered.

2.4 Summary

This section has given a brief background into CubeSats and ADCSs, as well as the theory and literature behind reaction wheels. The survey of existing reaction wheels makes clear the high cost of COTS products and inadequacy of the only other existing open-source design for use in orbit. This research indicates that there is sufficient motivation to develop an new open-source RWS, informed by the research carried out in the latter half of this chapter.

Chapter 3

Design Overview

This chapter gives an in-depth description of the open-source RWS design with justifications for the design decisions made. This chapter is divided into four sections: mechanical design, electronics, software, and supporting systems.

3.1 Mechanical Design

3.1.1 Design Decisions

Several mechanical design decisions were made for the RWS design, and are outlined below.

Wheel Arrangement Given the open-source nature of the project, the probability of a motor failure is likely to be higher than in a commercial RWS. To account for this, a four-wheel pyramidal arrangement was chosen due to its ability to continue functioning in the event of a single reaction wheel failure.

Tilt Angle Reaction wheels are designed to have a high moment of inertia with as low a mass as possible, resulting in it being shorter along its axis of rotation than its

other two axes. Given this geometry, the higher the angle β , the more difficult it is to arrange the reaction wheels to fit on a CubeSat board. Thus, to maximise the RWS's ability to modify β angle in future designs, a tilt angle of 35.26° was chosen, the highest a CubeSat RWS would reasonably require. Furthermore, the volume of the RWS with supporting hardware (e.g. batteries, attitude sensors, etc.) measured just over 1U, so the tilt angle of 35.26° suited the testing and verification of the design. Additionally, to accommodate future changes, the motor mounting structure was designed in such a way that the tilt angle can be easily adjusted with minimal design modifications.

Motor Selection The motors for the RWS were chosen based on the following requirements:

- Brushless DC (BLDC) - BLDC motors do not require brushes unlike conventional DC motors, thus have both increased durability and energy efficiency. Additionally, they offer high power at a low weight and can operate at very high speeds. For these reasons BLDC motors are almost exclusively used for reaction wheels.
- Torque and Maximum Speed - from Table 2.2 (Section 2.2.2), it was found that commercial reaction wheels had a maximum torque of 0.635-7mNm and a maximum speed of 6000-10000rpm. It was required that the selected motor had specifications similar to these.
- Small Size - the selected motor had to be small enough to fit four reaction wheels on a CubeSat board.
- Motor Quality - the selected motor was required to be highly reliable and durable both in Earth and space environments.

Based on the above requirements, BLDC motors were selected from Maxon and Faulhaber for their high quality motors. From among their motor ranges, both the Maxon EC20 Flat 351005 and the Faulhaber 2610B-SC motors met the RWS motor requirements (shown in Figure 3.1), including optional upgrades for extended temperature ratings for use in space, and vacuum-rated lubricant. Of these two, the 2610B-SC was

found to be a more suitable reaction wheel motor due to its low height, better cable placement and containing an in-built speed controller, which removed the need to develop separate BLDC motor driving circuits. The 2610B-SC motor datasheet can be found in Appendix E.

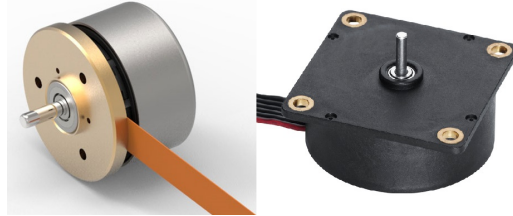


Figure 3.1: Maxon EC20 Flat 351005 and Faulhaber 2610B-SC Motors. Reproduced from [11] and [12].

Material and Manufacturing Method Laser cut acrylic was used to manufacture the motor mounts and mounting plate. This method allows for parts not only to be made and redesigned at a low cost, but also to have a very rapid manufacture time (around 10 minutes) with minimal physical effort or skill. Furthermore, this method allows for the same components to be laser cut from plate aluminium in future designs if additional structural strength is required. Aluminium was used for the wheels given its standard use in commercial reaction wheels.

3.1.2 Component Overview

A render of the assembled RWS is shown in 3.2. Each unit within the mechanical design is described below, with mechanical drawings of individual components found in Appendix A.

Wheel The aluminium wheel was designed to maximise its moment of inertia while minimising its mass and vertical height. As such, the wheel was shaped with the majority of its mass as far from the centre as possible as shown in Figure 3.3, resulting in a MOI of $7.32\text{E-}06\text{kg m}^2$ with a mass of 21.2g. The wheel was designed with sufficient

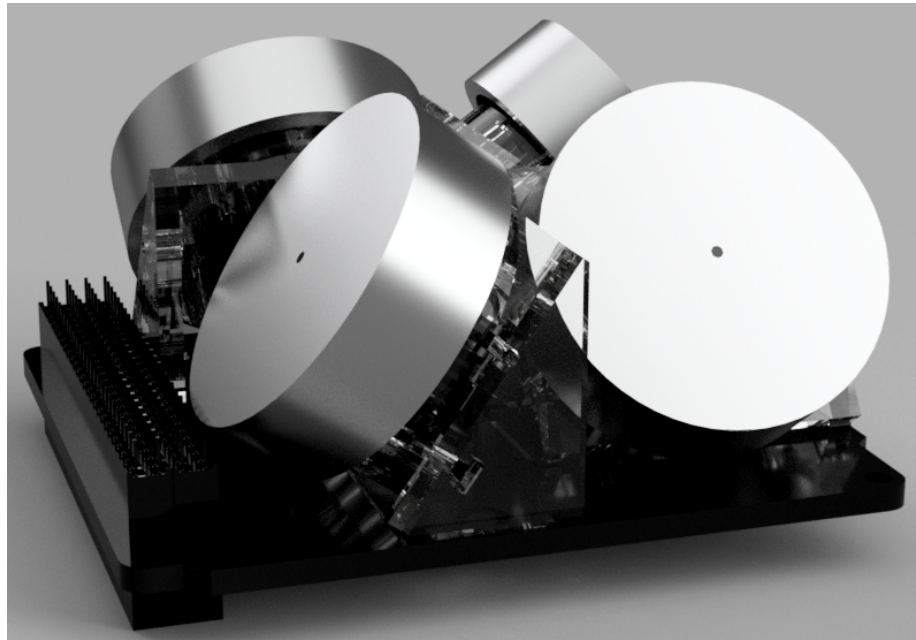


Figure 3.2: Render of the Assembled RWS

space in the centre to encapsulate the motor and was secured to the motor shaft using simple epoxy glue.

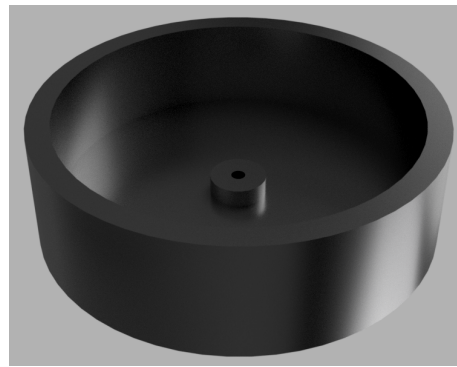


Figure 3.3: Render of Aluminium Wheel

Motor Mounts The motor mounts were designed to hold the motor secure at a tilt angle of 35.26° , while allowing enough clearance for the aluminium wheel to spin around. The motor mount assembly is shown in Figure 3.4.



Figure 3.4: Photos of Motor Mount without Wheel (left) and with Wheel attached (right).

Mounting Plate The motor mounts attach to a mounting plate (seen as the black layer of perspex in Figure 3.5), which is separated by 2mm from the motor driving electronics. This separation of electrical and mechanical components was made for several reasons. Firstly, this enables the RWS to be modular with low coupling between the mechanical and electrical systems, allowing each system to be developed largely independently of each other. Secondly, having a separation between each system reduces the vibrations from the reaction wheels transferred to the electronics. Holes were made in both the mounting plate and the PCB to allow the motor cables to pass through to their controller circuits.

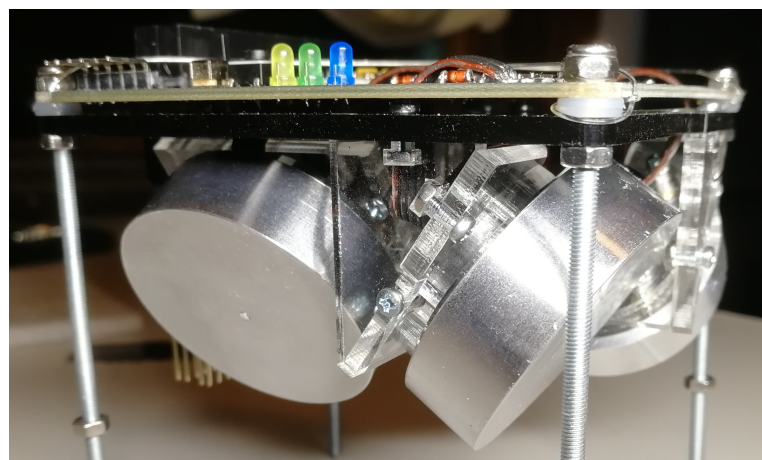


Figure 3.5: Photo of Assembled RWS

When the motors were arranged on the mounting board, there was sufficient space for

the CubeSat PC/104 header to fit through, so it was decided to let the header from the PCB pass through the mounting plate. This allows further systems to be connected below the RWS and removes the restriction of having the RWS to be mounted at the end of a CubeSat. Additionally, the mounting plate was placed upside down underneath the PCB to allow the two to be easily separated once the header pins were soldered onto the PCB.

3.2 Electrical Design

3.2.1 Overview

The RWS electronics are contained on a single CubeSat PCB, shown as a block diagram in Figure 3.6. A message is transmitted from the I₂C master over the I₂C bus to the microprocessor. This message contains the required orientation and spin of the satellite, as well as its current orientation and spin. The microprocessor calculates the required angular velocities to drive the motors and sends out pulse-width modulation (PWM) signal for each motor proportional to its commanded speed. The PWM signal is converted into an analog signal with a maximum voltage of 7.4V. As the motor spins, it sends out a pulse proportional to its rate of rotation. This pulse signal is converted in a frequency to voltage circuit, which outputs an analog signal proportional to the frequency that it receives. Finally, this analog voltage is measured by the microprocessor and sent back along the I₂C bus to the I₂C master as feedback.

CubeSat power systems typically use Li-ion or Li-polymer batteries [40], most in a 2SnP arrangement which results in a raw battery output of 7.4V. This value was used as the power supply voltage to drive motors, although any voltage from 1.7-18V can be used to power the 2610B-SC motor.

Each block is explained below, with full schematics included in Appendix B.

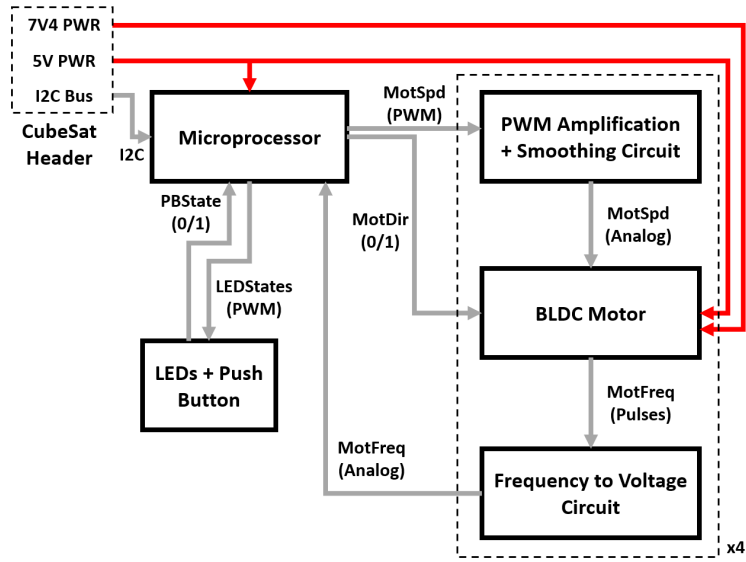


Figure 3.6: Block Diagram of RWS Electronics

Microprocessor For the microprocessor, an Arduino Pro Mini was chosen due to the ease of software development and its small footprint size. A schematic showing the connectivity to the Arduino is shown in Figure 3.7 and its software is covered in Section 3.4.

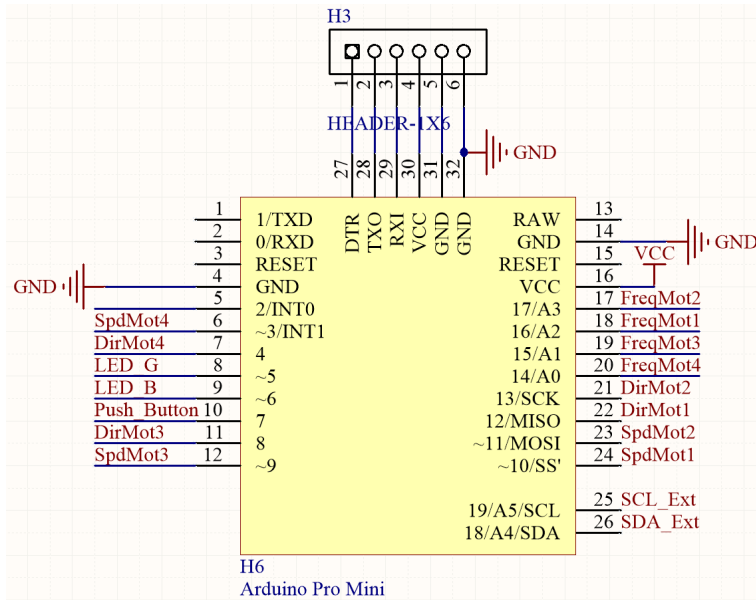


Figure 3.7: Schematic of Arduino Connectivity

PWM Amplification and Smoothing Circuit The PWM amplification and smoothing circuit (Figure 3.8) converts a 5V PWM signal to an analog signal with a range of 0V to 7.4V (Figure 3.9). Amplification is done to make use of the full speed range of the 2610B-SC motor, which runs at full speed when the input speed signal is equal to M_VIN (see paragraph ‘BLDC Motor’ below). The PWM signal is smoothed to produce an analog signal in order to eliminate unnecessary acceleration and braking of the motor that a PWM signal would produce.

The first transistor (Q1) amplifies the 5V PWM signal from the Arduino to a 7.4V PWM signal. This signal is then smoothed by an RC filter (R3 and C3) to create an analog (non-pulsed) signal which drives a second transistor (Q2) to decrease nonlinearity between the circuit’s input and output. Due to its simplicity, the circuit inverts the input signal, but this can be easily adjusted for in software. A pullup resistor is added to the input pin to set the motor speed to zero in the case of a power failure in the microprocessor.

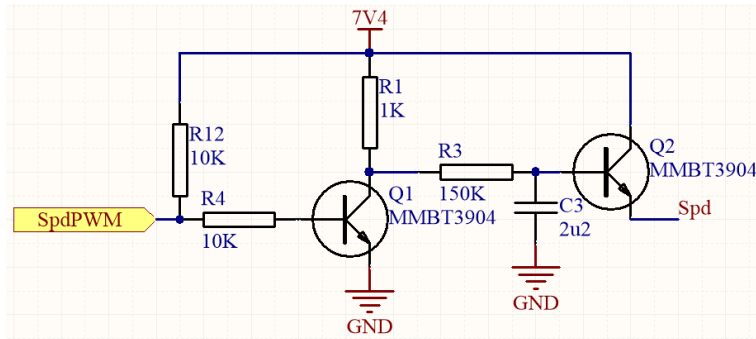


Figure 3.8: Schematic of PWM Amplification and Smoothing Circuit

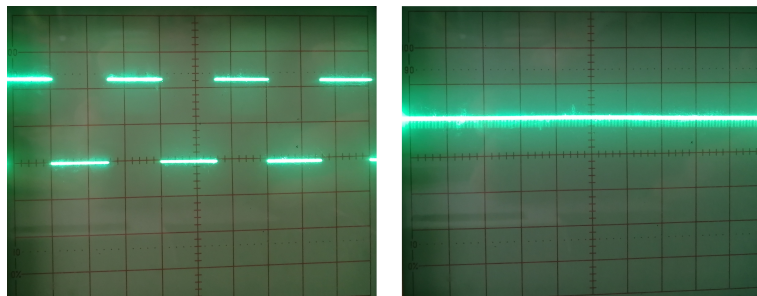


Figure 3.9: PWM Circuit Input and Output Signals

BLDC Motor To connect the motor to the PCB, the motor cable is soldered to six exposed pads (at the centre of Figure 3.10). These pads are:

- E_VIN - power supply for motor electronics
- M_VIN - power supply for driving motor
- GND - ground
- SPD - for controlling speed of motor, between 0V (stopped) and M_VIN (full speed)
- DIR - for controlling direction of motor, 0V (CCW) or E_VIN (CW)
- FRQ - output from the motor, giving six pulses (0-E_VIN) every rotation

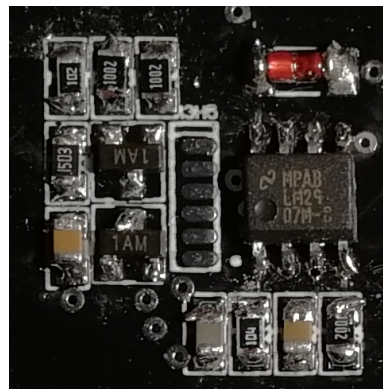


Figure 3.10: Photo of Motor Circuit

Frequency to Voltage Circuit The frequency to voltage circuit (Figure 3.11) converts a pulsed signal to an analog voltage proportional to the frequency of pulses in the input signal. This is done to provide feedback to the microcontroller, allowing it to ensure that the reaction wheels are functioning correctly. The circuit can also be used to provide data in calculating a satellite's attitude if required (e.g. in a Kalman filter). The circuit is taken directly from the LM2907 chip's datasheet, with the exception of the diode (D4) connecting the chip's ground to the PCB ground. This change was made as the LM2907 requires a zero-crossing frequency signal (i.e. a signal alternating

between positive and negative voltages). As the motor cannot produce a negative voltage signal, a diode was added to raise the chip's 'ground' to 0.7V relative to the PCB and the motor.

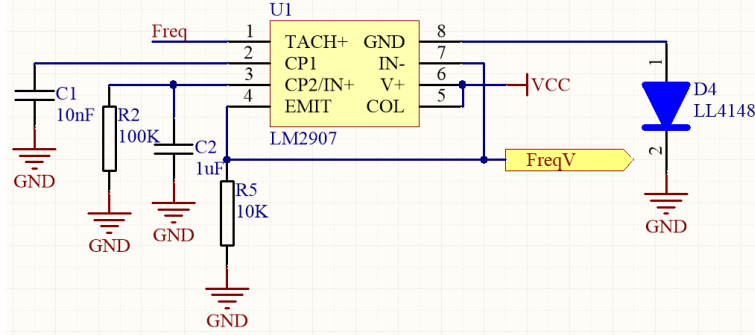


Figure 3.11: Schematic of Frequency to Voltage Circuit

LEDs and Push Button LEDs and a push button were included to assist with debugging and software development, as well as a slide switch to control power to the board. Note that these would not normally be included on a flight model.

3.3 Hardware Cost Breakdown

Table 3.1 gives the cost breakdown of parts and materials used in the construction of the RWS. The total cost of the RWS amounts to under \$1000, minus the cost of manufacturing time and equipment.

Table 3.1: Cost Breakdown of RWS Hardware

Items	Cost (AUD\$)
Electrical Components	61
PCB	20
Motors (x4)	770
Perspex Sheets	13
Mechanical Fasteners	57
Aluminium Round Bar (est.)	25
Total	946

3.4 Microprocessor Software

Software on the microprocessor consists of two main tasks - the controller task and wheel distribution. Note that since the focus of this thesis was on hardware development and testing, software was not written for a space environment (with three axes of freedom), but rather to demonstrate basic RWS functionality (on Earth) to show that the hardware could potentially function adequately in space given a more refined software package.

3.4.1 Controller Task

The controller task is responsible for calculating the total required angular momentum to reach the target attitude and spin, given the current attitude and spin. This was split into two modes as described below.

Detumbling The first controller mode is to detumble, or to reduce angular velocity to zero around all axes. A simple P controller was found to be sufficient for this task, given as:

$$\mathbf{E} = \mathbf{0} - \boldsymbol{\omega}_{\mathbf{B}}$$

$$d\mathbf{H}_{\mathbf{B}} = P \times \mathbf{E}$$

where \mathbf{E} is the error to be minimised, $\boldsymbol{\omega}_{\mathbf{B}}$ is the satellite's angular velocity, $d\mathbf{H}_{\mathbf{B}}$ is the required change in total angular momentum and P is some tuned constant.

Pointing The second controller mode is to point and halt at a specified orientation. Since the testing methods available only allowed a single axis of rotation, the pointing controller was written as a PD controller for single-axis rotation, given as:

$$E = \theta_{targ} - \theta_B$$

$$dH_B = P \times E + D \times \omega_B$$

where θ_{targ} and θ_B are the target and current angles of rotation around the axis of rotation, and D is a tuned constant.

These controllers were both built and tested within a MATLAB simulation to facilitate software development before the prototype was completed. Figure 3.12 shows the pointing algorithm running in the simulation.

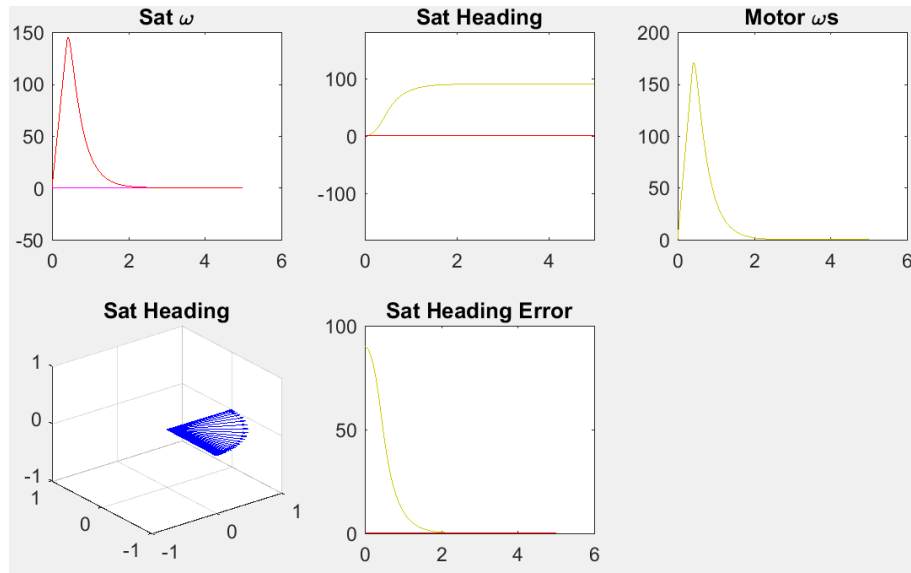


Figure 3.12: Simulation Running Pointing Algorithm (0-90°)

3.4.2 Wheel Distribution

Wheel distribution was split into two components - the pseudoinverse distribution and motor limiting.

Pseudoinverse Distribution From Section 2.3.3 the pseudoinverse distribution was chosen due to its ease of implementation and low processing cost. With a tilt angle of

35.26°, the distribution of total angular momentum to the four wheels is given by:

$$\mathbf{H}_W = \frac{\sqrt{3}}{4} \times \begin{bmatrix} 0 & \sqrt{2} & -1 \\ -\sqrt{2} & 0 & -1 \\ 0 & -\sqrt{2} & -1 \\ \sqrt{2} & 0 & -1 \end{bmatrix} \mathbf{H}_B$$

which is converted to angular velocities by simply $\omega_W = \mathbf{H}_W / I$ where I is the combined moment of inertia of the wheel and motor rotor, equal to 1.411E-05kg m².

Motor Limiting In order to obtain a linear response from the motors, software limits were put in place to prevent commands from passing the physical limits of the motors. Limits were put on the maximum change in speed (corresponding to the motor's torque limit), and an upper bound were placed on speed of the motors. Motor speeds were also given a lower bound due to the non-linear behaviour inherent to BLDC motors at near-zero speeds.

3.5 Supporting Hardware

To test the RWS, some basic satellite functionality was required, namely:

- On-board power supply and monitoring
- Attitude and spin determination
- Data logging facilities
- Wireless external control

Three PCBs were designed to meet these requirements, with total costs for supporting hardware amounting to \$107. The connectivity of the satellite is shown as a block diagram in Figure 3.13 and described below. Detailed schematics of these boards can be found in Appendix C.

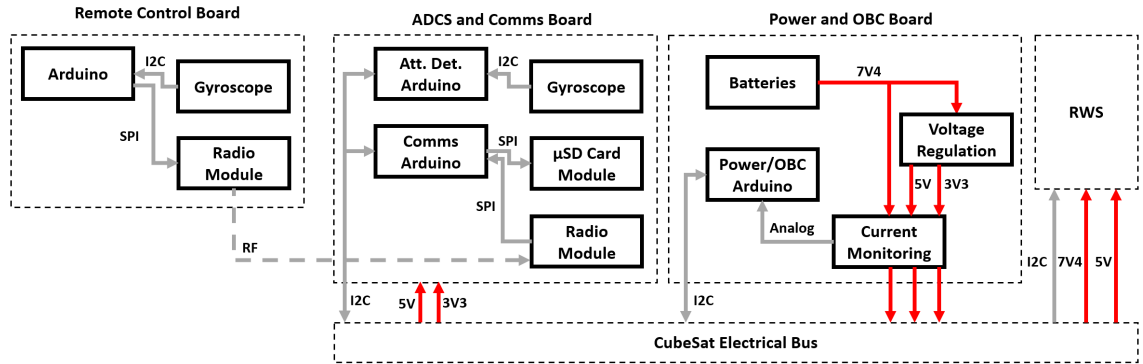


Figure 3.13: Block Diagram of Satellite Electronics

Remote Control Board Acting as a ground station, this board provides a wireless link to the RWS via the Communications Arduino, allowing commands to be sent during runtime, such as ‘detumble’ or ‘point at angle x’. The target angle that was transmitted was able to be adjusted via serial communications from a computer, or by using the remote control board’s heading tracked by a gyroscope.

ADCS and Communications Board This board contains two Arduinos with different functions. The attitude determination Arduino polls a gyroscope and calculates the satellite’s heading as a quaternion (to avoid gimbal locks). Attitude and spin data is then transmitted to the RWS. The communications board passes received RF messages to the RWS, as well as logging telemetry data being generated by the satellite to a microSD card, including:

- RF messages received
- Attitude and spin data
- RWS wheel speeds
- Current draw from power lines

Power and On-Board Computer Board This board is responsible for regulating, monitoring and distributing power to the other CubeSat boards. Two sets of 5xAA

batteries are used for power generation - one set is regulated to 5V and 3.3V, while the other set is used exclusively to power the RWS motors. Each power rail has a current monitoring circuit which lets the power Arduino measure current draw. Additionally, the power Arduino acts as the I2C master and manages data flow around the satellite.

The fully assembled RWS with supporting satellite hardware can be seen in Figure 3.14

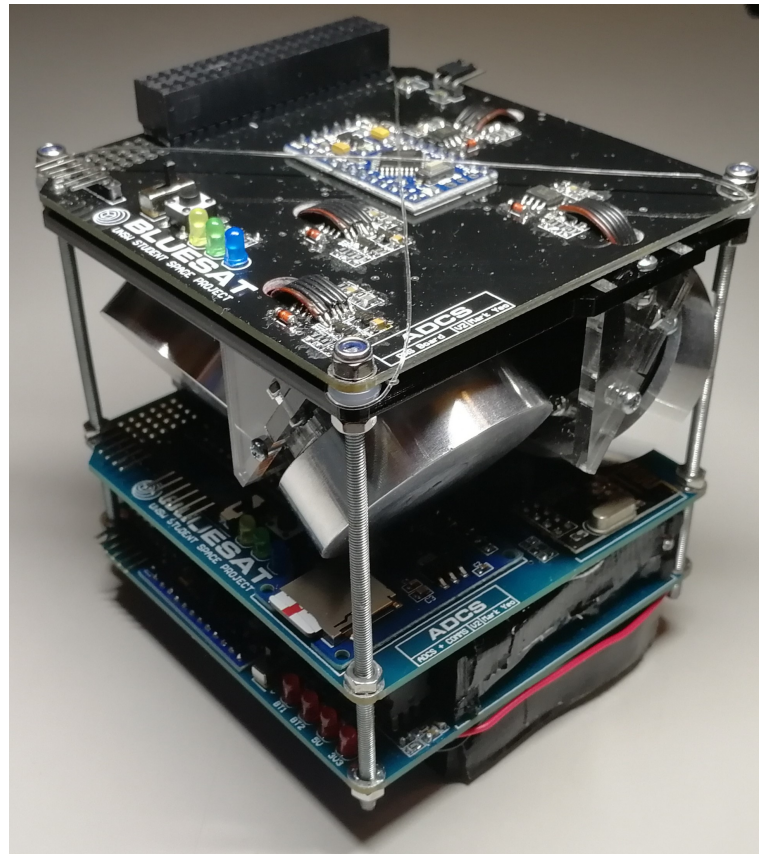


Figure 3.14: Photo of Assembled Satellite

Chapter 4

Performance Testing and Results

This section covers the testing carried out to evaluate the performance of the RWS prototype. Performance was tested in terms of the RWS's ability to detumble and point, as well as its capacity to store angular momentum. These aspects were tested using two setups. The first setup involved using a spherical cap air bearing which freely allowed single-axis rotation with minimal friction, making it suited for testing detumbling and pointing functionality. The second method involved suspending the RWS at the bottom of a stairwell. The long length of string allowed for single axis rotation with a very small restoring torque, and allowed for testing algorithms without the additional MOI of the air bearing bowl. This made this setup well suited for evaluating the RWS's momentum storage capacity. As both methods allowed only single-axis rotation, multiple tests were run with the RWS mounted in different orientations.

4.1 Detumbling Performance

To evaluate detumbling performance, the RWS was placed on an air bearing as shown in Figure 4.1. (The air bearing datasheet can be found in Appendix E). An initial spin was imparted by hand on the RWS, after which a control signal was sent wirelessly to trigger the detumbling software. To obtain results within the reaction wheels' linear

range, initial motor speeds were set to half of their maximum speed (550rad/s). Figure D.6 graphs the telemetry data collected from detumbling after an initial spin in the positive Z direction (counter-clockwise around the positive Z axis).

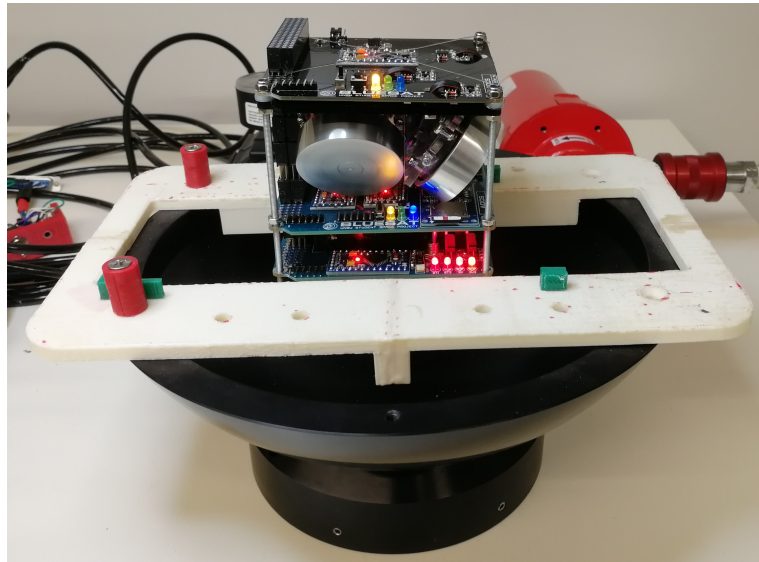


Figure 4.1: Air Bearing Setup for Z-Axis Testing

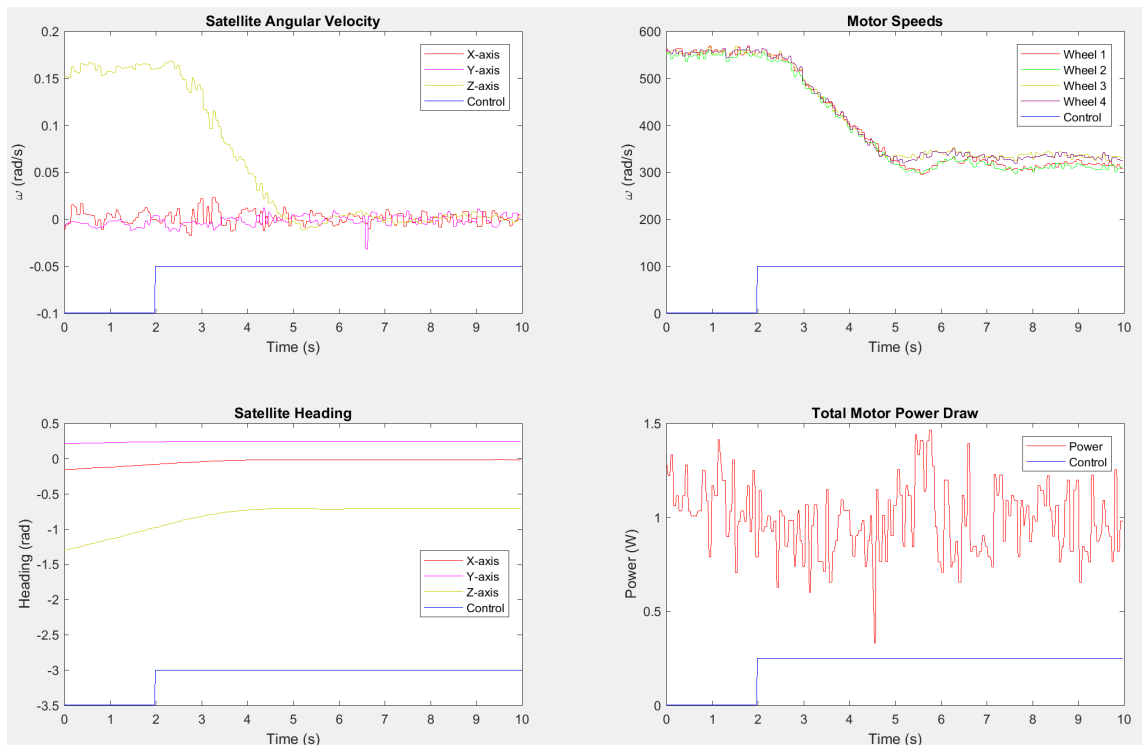


Figure 4.2: Detumble Performance around Z+ Axis

From this data, the decrease in the satellite's angular velocity around the Z axis can clearly be seen, taking about four seconds for it to drop to a small steady state value. Of note was a significant 'wobble' along the X and Y axes which was not minimised. This was likely due to having a single P value shared across the X,Y and Z P-controllers, coupled with the air bearing bowl having fairly different MOIs around its X and Y axes (19g.m^2) compared to around its Z axis (13g.m^2). Also of note was that motor power draw was largely independent of both motor speeds and braking (decreasing motor speed).

The same experiment was run again, but with the initial spin along the negative Z axis. Results show very similar results to the previous test, as shown in Figure D.7. Unlike the previous test however, a power spike was observed as the motors applied torque to increase motor speed.

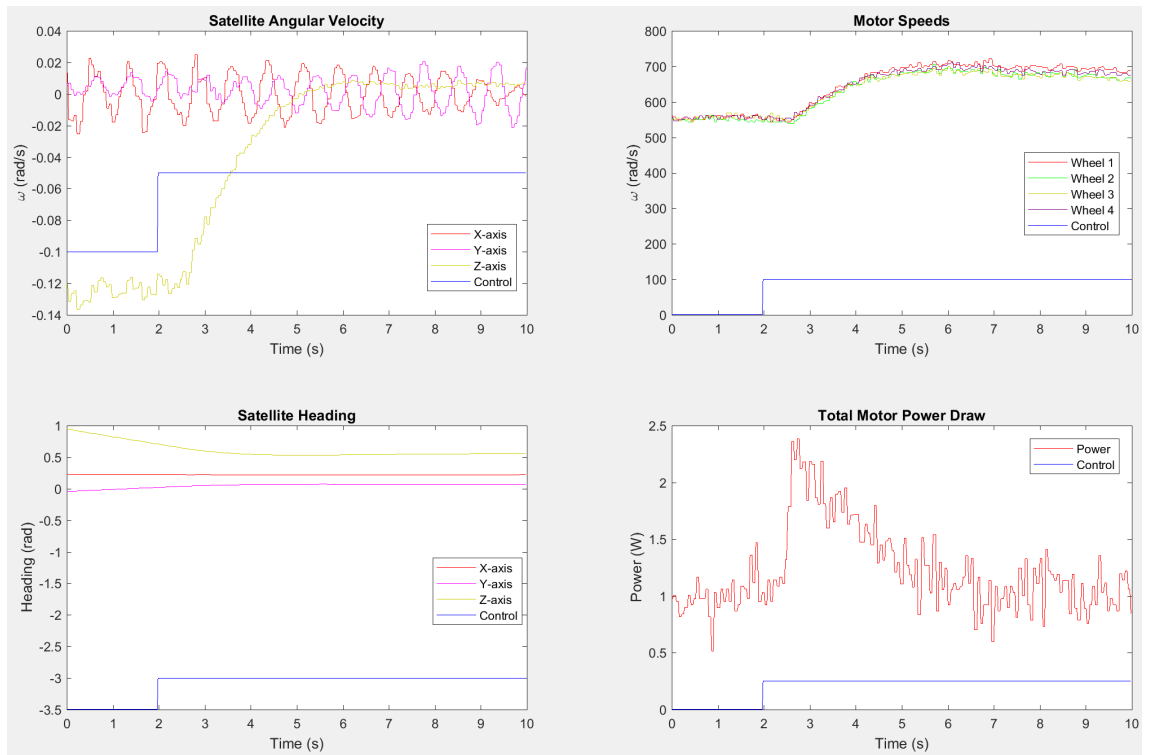


Figure 4.3: Detumble Performance around Z- Axis

These two experiments were run multiple times with the satellite oriented in different orientations to allow testing in the X and Y directions. These experiments gave very

similar results to those shown above, with all results contained in Appendix D. Tests were also done in the XY direction, as shown in Figures 4.4-D.9.

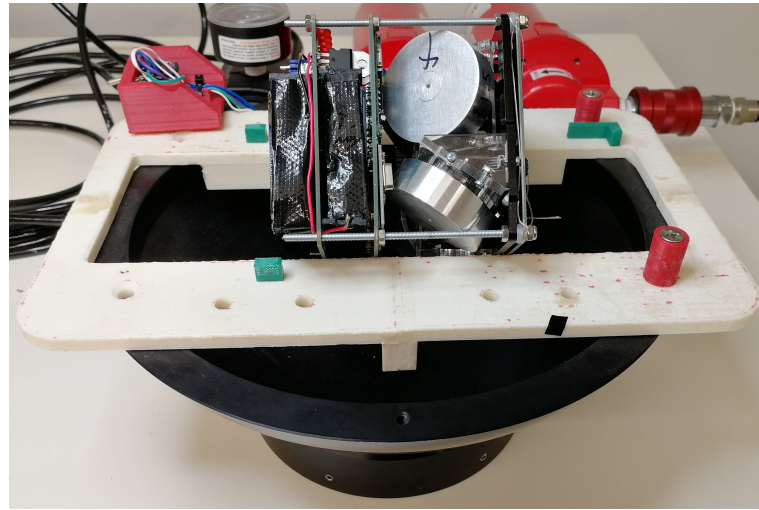


Figure 4.4: Air Bearing Setup for X+Y+ Axis Testing

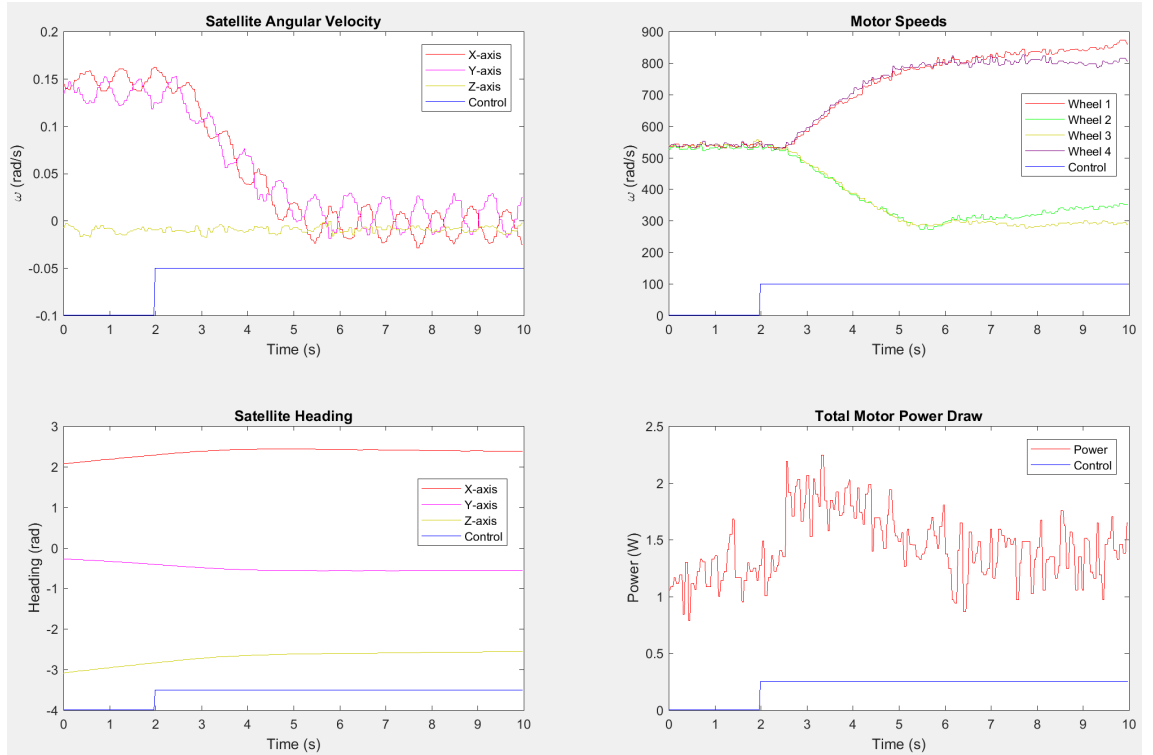


Figure 4.5: Detumble Performance around X+Y+ Axis

With this orientation, substantial 'wobble' was observed in both X and Y axes after detumbling. This may possibly be due to the uneven momentum space generated by

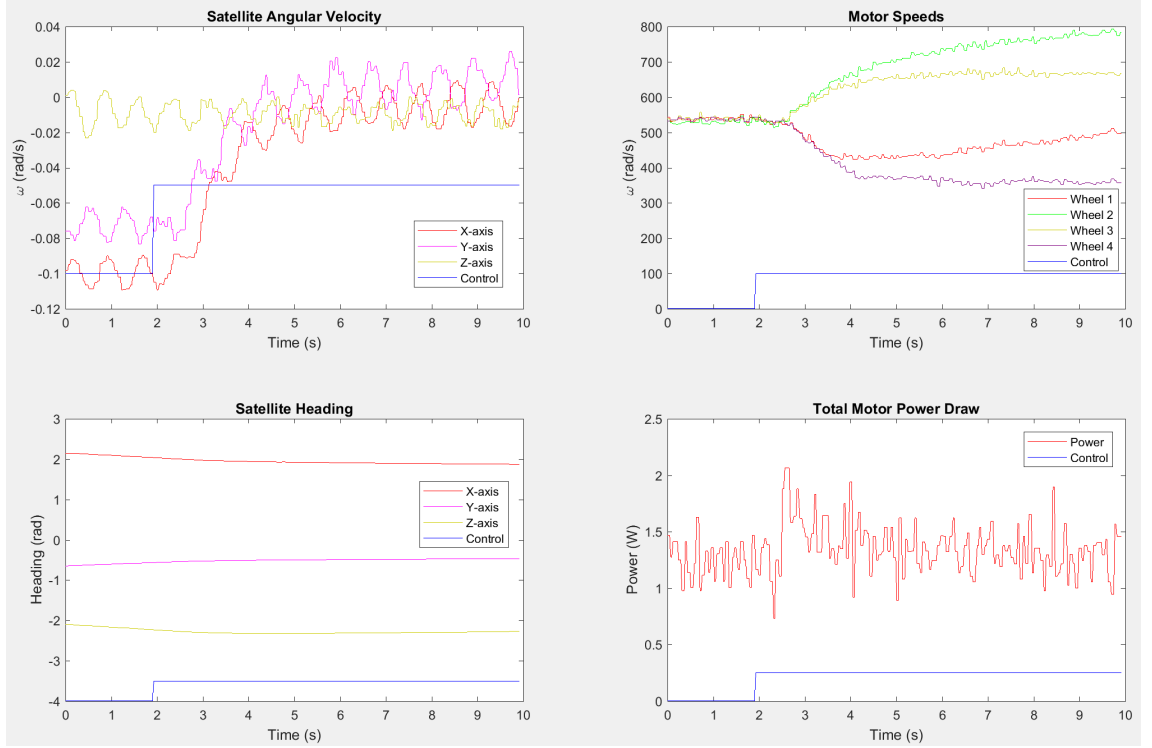


Figure 4.6: Detumble Performance around X-Y- Axis

the pseudoinverse distribution law, causing performance in some axes to be different from others (see Figure 2.8 in Section 2.3.3).

4.2 Pointing Performance

To evaluate pointing performance, the RWS was placed stationary on the air bearing with a heading of -90° , then target angles of $+180^\circ$ followed by -90° were commanded via the RF link. Figure D.12 shows pointing data for rotation around the Z axis.

From the pointing data, it can be seen that pointing performance is fairly accurate and has a fast response in both clockwise and anticlockwise adjustments, especially given the added MOI of the air bearing bowl. Note that the shortest route was chosen when $+180^\circ$ was commanded as the target angle.

This test was extended to test if motor saturation would occur through multiple point-

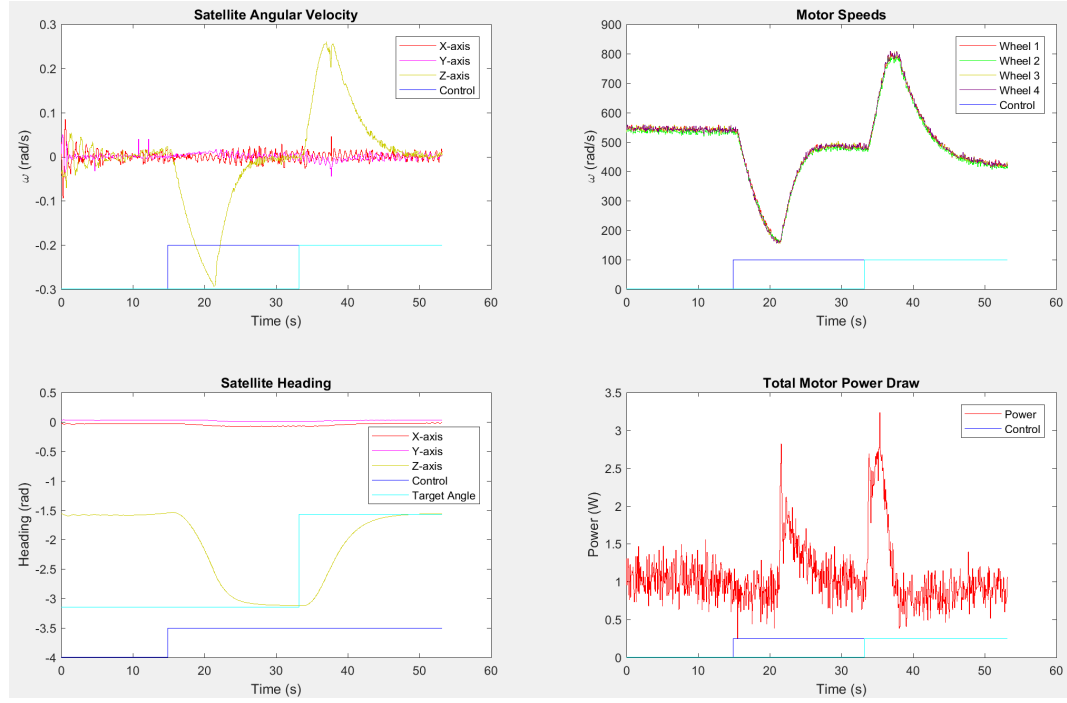


Figure 4.7: Pointing Performance around Z Axis.
Note that the target angle of $+180^\circ$ is shown as -180° for ease of reading.

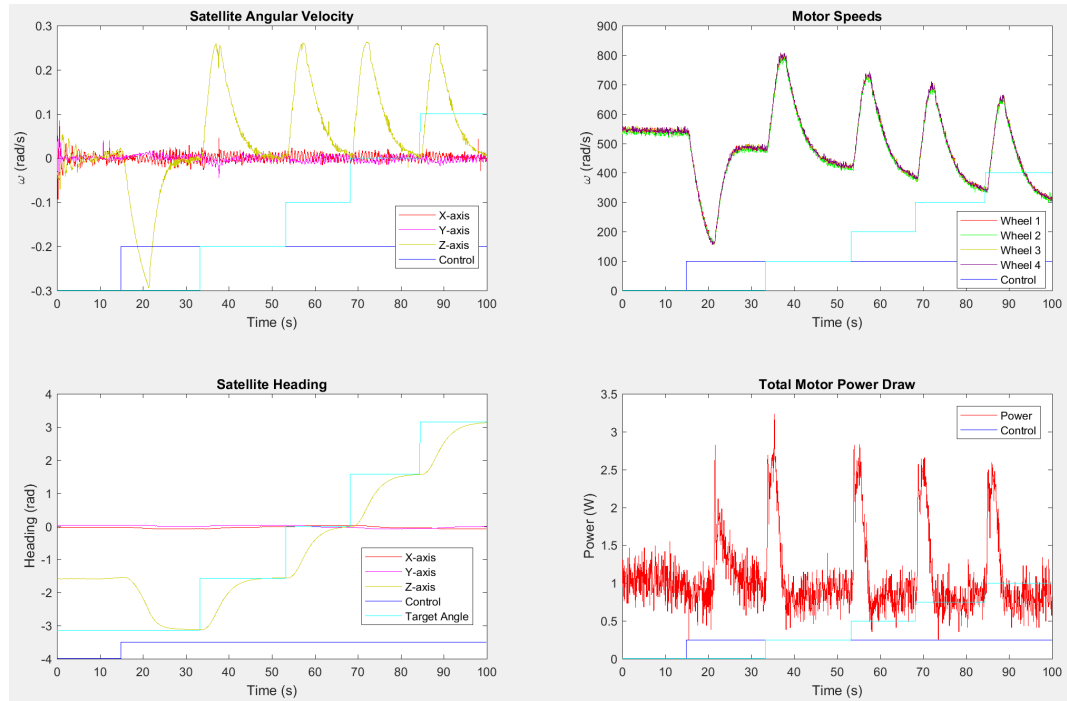


Figure 4.8: Pointing Performance around Z Axis (Extended)

ing commands, as shown in Figure D.13. Interestingly the steady-state motor speed decreased over time, suggesting that momentum was being dumped somewhere in the testing system. This is unlikely to be due to friction in the air bearing (see Figure D.1), although other effects may be the cause such as vibrations caused by motors or precession.

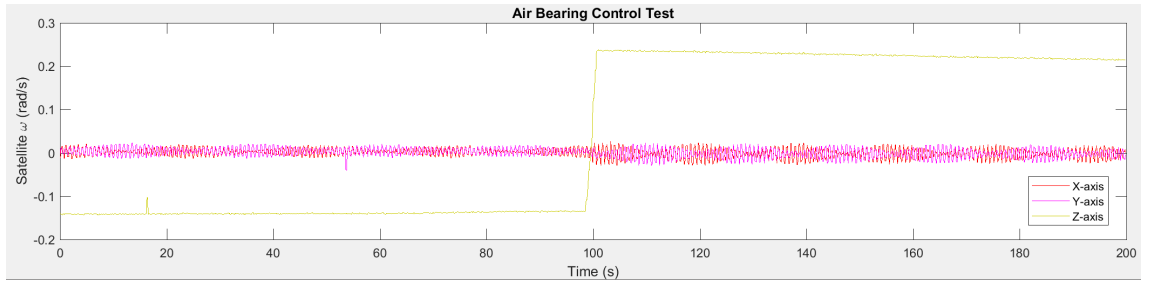


Figure 4.9: Air Bearing Natural Spin Decay.
Note that spin was manually reversed at 100s

As with detumbling, pointing was tested in multiple orientations. Performance in other axes were very similar to that shown above, and can be found in Appendix D.

4.3 Momentum Storage Capacity

To determine momentum storage capacity, the RWS was suspended by 20m of nylon fishing line in a stairwell (Figure 4.10). The RWS was then spun at a high enough rate that the motors saturated when commanded to detumble. From this experiment the momentum storage capacity of the RWS was able to be calculated.

MOI Estimation To estimate its MOIs, the RWS was estimated as a homogenous prism of mass 0.672kg with side lengths {97,87,92}mm in the X, Y and Z directions respectively. The MOIs in X, Y and Z were calculated to be {9.0E-04,1.0E-03,9.5E-04}kg.m² respectively. To confirm the order of magnitude of this estimation, the RWS was suspended on a shorter length of fishing line and the oscillation period was measured. This was compared to the oscillation period of a well-defined object - an aluminium bar of mass 52g with side lengths 16,459,3, with a calculated MOI of 9.13E-



Figure 4.10: Setup for Stairwell Suspension Test

04kg.m^2 . The oscillation periods were within 5% of one another, confirming that the MOI estimations were reasonably close to the actual MOIs.

Figure D.16 shows results of the stairwell experiment around the Z axis. Note that the restoring torque of the line on the RWS was non-zero but negligible in these tests, as shown in Figure 4.12.

From the experiment it was measured that the RWS was able to reduce the satellite's ω in both directions (combined) by roughly 13rad/s . Thus, the momentum capacity in the Z direction was calculated to be $I \times \omega = 1.2E - 02\text{kg.m}^2\text{s} = 12\text{mNm s}$. The experiment was repeated for the X and Y axes (data found in Appendix D), giving moment capacities of 3mNm s and 2.8mNm s respectively. This difference between momentum capacities around the Z axis and the X/Y axes is likely due to the pyramid configuration, which gives a larger maximum momentum storages around the Z axis compared to the X/Y axes (see paragraph below).

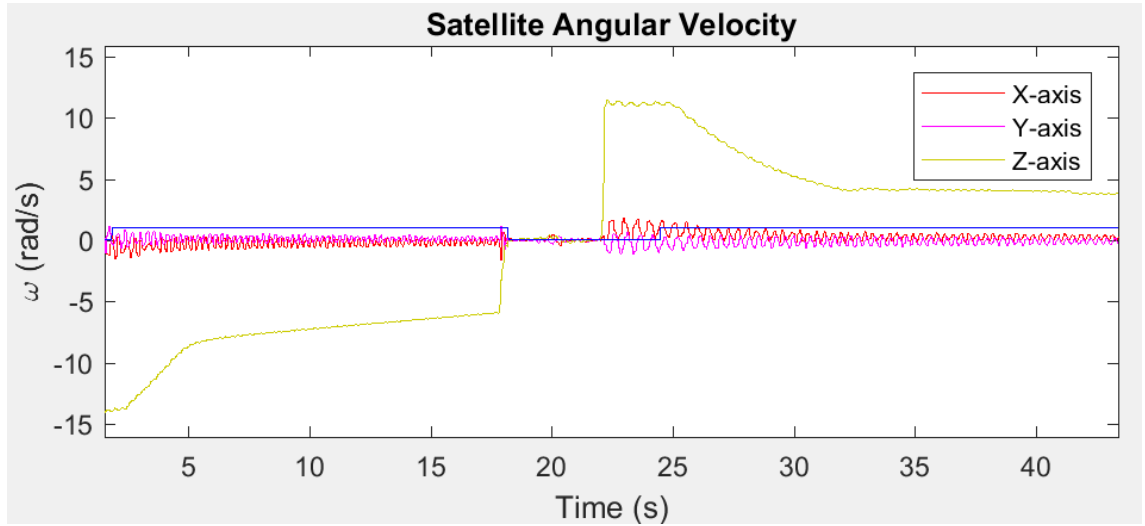
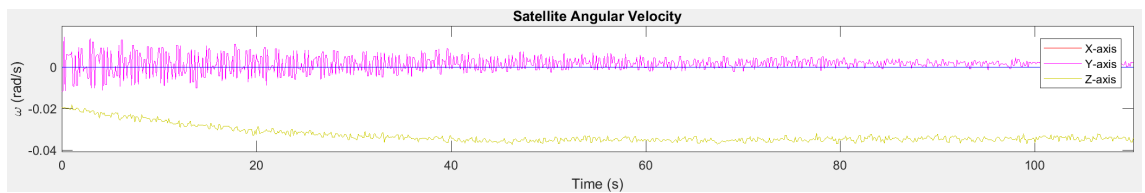


Figure 4.11: Momentum Capacity around Z Axis

Figure 4.12: Effect of Restoring Torque on Satellite ω

Theoretical Maximum Momentum Storage To calculate the theoretical maximum momentum storage, we consider the maximum motor speed (1392.8 rad/s) and the motor/wheel MOI ($1.4100\text{e-}05 \text{ kg.m}^2$), which gives a maximum momentum storage of 19.6mNms per wheel. In the RWS's pyramid array this amounts to a maximum momentum storage of {32.0, 32.0, 45.3}mNms around the X, Y and Z axes respectively. This theoretical maximum is substantially larger than those found by experiment - this difference is likely due to a combination of limits with the pseudoinverse method, errors in MOI estimation and possibly precession effects of the already-spinning wheels adding to the MOI of the satellite.

4.4 Power Draw

To measure power draw, the RWS was commanded to spin its motors at specified speeds while the current and voltage levels were logged. Figure D.21 shows the power draw when all four wheels were commanded to spin from rest to full speed, back down to zero. Note that the 8.2W peak is determined by the maximum amount of torque applied by the motor speed controller, and can be regulated in software by applying a lower torque over a longer period of time.

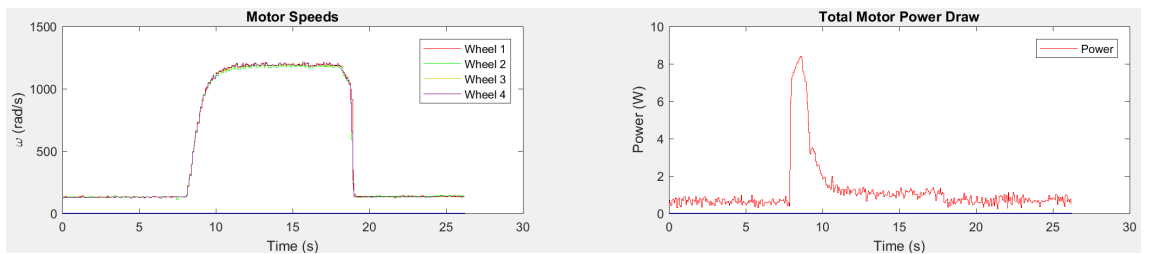


Figure 4.13: Motor Power Draw from Zero to Full Speed with Maximum Acceleration

Additional tests were run at different speeds (data found in Appendix D), with the results summarised in Table 4.1.

Table 4.1: RWS Power Draws

Motor Speed	Ave. Power Draw (W)
0 rad/s	0.9
150 rad/s (Minimum Linear Speed)	0.8
700 rad/s (Medium Linear Speed)	1.0
1400 rad/s (Max Speed)	1.2
Max Acceleration	8.2

Of interest in particular is the relatively high power draws for holding constant speeds, especially when motors were halted. This may be due to various factors, such as power losses along PCB traces between the batteries and motor, power draw by the speed controller, uneven loads from motor vibrations, or jitter in the speed control signal (resulting in the motor constantly accelerating then braking). The latter two factors may also be the cause in the high variance of the power draw signal.

Chapter 5

Comparison of RWS with Existing Designs

This section compares the specifications and performance of the prototype RWS with existing designs.

5.1 Comparison of Specifications

Table 5.1 compares the specifications of individual COTS reaction wheels (from Table 2.2 in Section 2) to the reaction wheels used in the prototype RWS. It can be seen that the prototype reaction wheel (motor, wheel and motor mounting structure) fits cleanly within the typical range of COTS specifications, with the exception of a slightly higher maximum speed and at a substantially lower price. The prototype reaction wheel also has a lower mass, but this is expected to rise if perspex is swapped for aluminium plate and if the reaction wheels are encapsulated.

Table 5.2 gives a summary of specifications of COTS RWSs (where available)(from

Table 5.1: Comparison of Specifications of COTS and Prototype Reaction Wheels

Specification	COTS Value	Prototype Value
Torque (mNm)	0.635 - 7	4.8
Max Momentum (mNms)	10 - 50	19.6
Max Speed (rpm)	6000 - 10000	13300
Ave Power (W)	0.15 - 0.85	0.25
Mass (g)	110 - 250	52.5
Price (USD)	6385 - 7685	216

Table 2.3 in Section 2) compared with the prototype RWS. From the table it can be seen that the prototype RWS has fairly similar specifications to commercial products. Substantially lower momentum capacities were measured experimentally in the X and Y axes when compared to COTS RWSs (see Section 4.3 for related discussion). Additionally, the prototype's power draw was generally on the high end of COTS power draws (see Section 4.4 for related discussion). As was the case in the comparison against individual reaction wheels, the prototype RWS cost was substantially lower than commercial counterparts (see Section 2.2.3 for justification of commercial prices).

Table 5.2: Comparison of Specifications of COTS and Prototype Reaction Wheels
(where available).

Sources: [4][13][5][6][14]

Specification	COTS Value	Prototype Value
Torque (mNm)	{5.9,5.9,2.5}	{7.8,7.8,11.1} theoretical
Max Momentum (mNms)	{40.5,40.5,17.2}	{3.0,2.8,12.0} ({32.0, 32.0, 45.3} theoretical)
Min Power (W)	0.25 - 0.82	0.8
Ave Power (W)	0.8 - 1.4	0.9
Max Power (W)	6.4 - 7.0	8.0
Price (AUD\$)	19870 - 23160	946
Height (mm)	50.0 - 61.6	59.0
Mass (g)	236 - 940	338

5.2 Comparison of Design Features

This section compares major design differences between the prototype and COTS products other than those covered above.

5.2.1 Prototype Advantages

Advantages of the prototype RWS design compared to commercial products include the following.

CubeSat Headers As noted in Section 2.2.2, four-wheel COTS RWSs do not contain CubeSat PC/104 headers as the wheels take up the entire CubeSat cross-section. As such, satellites utilising these RWSs must place the module at either end of the satellite, as the CubeSat electrical bus cannot pass through the module. This is generally not an issue for performance as torque is translation-independent. However, CubeSats with two payloads each requiring end-face access or those seeking to minimise their MOIs may benefit from locating the RWS more towards the centre. In this regard, the prototype includes CubeSat headers to allow it to be placed anywhere along the CubeSat stack.

Adjustable Tilt Angle The RWS was designed such that the tilt angle of the wheels can be easily adjusted by redesigning a single part. This allows satellite developers to optimise the torque and momentum space to the attitude requirements of the mission, increases both attitude control performance and power efficiency.

Open-Source Design In addition to the above point, satellite developers can customise any aspect of the RWS design to suit their mission needs. For example, lighter wheels could be used for a mission without large momentum capacity requirements, or sensors integrated into the RWS PCB to form an integrated ADCS.

5.3 Prototype Disadvantages

Disadvantages of the prototype RWS design compared to commercial products include the following.

Non-encapsulated Reaction Wheels The majority of commercial reaction wheels and RWSs encapsulate each entire motor and wheel unit (see middle and right RWS in Figure 2.4 in Section 2.2.2. This is done to prevent reaction wheel failure from the introduction of any loose particles in the satellite during launch, as well as preventing damage to the rest of the satellite in the event that a rotating component dislodges or breaks off during operation. Due to the prototype nature of the current design, reaction wheel encapsulation was not considered although it could be easily added in future iterations.

Wheel Balancing Commercial reaction wheels are balanced during manufacturing, but require very precise machinery to manufacture and adjust wheel balance. Due to the tools available for prototype manufacturing, a press-fit was unavailable as an option to secure the aluminium wheels to the motor shafts, thus the wheels were glued onto the motors with epoxy. This introduced a small but noticeable unbalance with the wheels, especially when operating at higher speeds - this caused vibrations within the system and was likely a major source of energy inefficiency in the prototype. At the moment no alternatives can be found other than using higher precision tools, or simple trial-and-error.

5.4 Summary

This section compared the specifications and design features of the prototype RWS against COTS products. It was found that the prototype had very similar specifications to commercial designs, but had a higher power draw and much lower momentum capacities (likely due to systematic errors in testing). Additionally, the cost of the prototype was substantially lower than commercial products. The prototype also included some improvements on commercial designs such as adjustable tilt angles and the inclusion of the CubeSat header, but did not incorporate other useful features such as reaction wheel encapsulation and wheel balancing.

Chapter 6

Conclusions and Future Work

This thesis covered the background, design and performance results of a new open-source CubeSat RWS design. Research was carried out, showing that existing COTS RWS cost upwards of around \$20 000, placing them out of reach of many CubeSat developers with smaller budgets. It was also shown that the only existing open-source RWS was built for ground testing and overpowered for space applications, making further development for space unsuitable. This highlights a need for a new open-source CubeSat RWS to be designed, and forms the basis of this thesis.

This thesis's aim was to develop and test an open-source CubeSat reaction wheel system. A prototype RWS was designed and manufactured, with several design decisions based on existing products and relevant literature. Prototype testing showed reasonable performance in attitude control tasks, with its measured specifications closely matching commercial products. Key differences included the prototype having a slightly higher power draw, and a significantly lower momentum capacity - although the latter is likely to be due to systematic errors during testing. Additionally, the prototype cost amounted to just under \$1000, about 1/20th the price of commercial RWS modules. Design features were added to the prototype to allow customisation and optimisation of the design to suit the mission at hand. However, a few beneficial features were not included or unable to be achieved, although these problems may be solved in future

design iterations and with more precise manufacturing methods.

Future work on the RWS design includes but is not limited to the following:

- Improving RWS electronics - RWS electronics may be improved by adding individual power control circuits for each motor to be used in the event of motor failure or overcurrent, and by redesigning the RWS electronics using components with space-heritage to increase circuit reliability in space.
- Analysing motor performance - To allow complete control over each motor's speed and acceleration, the motors could be replaced with the Faulhaber 2610B (equivalent motor without an integrated speed controller) and driven with dedicated motor driving circuits on the RWS PCB. Additionally, further analysis could be carried out as to the optimum voltage level for driving motors so as to minimise power draw.
- Optimising wheel geometry - the aluminium wheel geometry can be further optimised to maximise its MOI while keeping below a mass and volume budget and maintaining structural integrity
- Analysis of mechanical structure - the RWS's mechanical structure will need to be analysed (e.g. using finite-element analysis) to ensure that it will be able to withstand forces and vibrations during launch.
- Improving RWS software - the current software was written to demonstrate basic attitude control functionality in a testing environment. There is a lot of room for testing performance to be improved, as well as developing software for the RWS to operate in orbit with three-axes of rotational freedom.

Overall, the RWS prototype has demonstrated performance comparable to commercial products at a significantly lower price, and through future development and testing, this open-source design has the potential to provide satellite developers with a low-cost yet reliable CubeSat reaction wheel system. All code and design files for this project can be found online at <https://bitbucket.org/bluesat/cubesat-adcs>.

Bibliography

- [1] UNSW. UNSW in thrilling rescue of lost' Aussie satellites, 2017.
- [2] ITU. ITUpSat-1.
- [3] James R. Wertz and Wiley Larson. *B3 - Space Mission Analysis and Design*. 1999.
- [4] Clyde Space. Attitude Determination and Control System.
- [5] GOMspace. NanoTorque GSW-600.
- [6] Nano Avionics. CubeSat Reaction Wheels Control System "SatBus 4RW".
- [7] Jeremy A. Louke, Erin S. Schmidt, and Calvin J. Young. An Open-Source Reaction Wheel System for Oregon's First Satellite. *Aiaa Space 2016*, (September):1–7, 2016.
- [8] F Landis Markley and John L Crassidis. *Fundamentals of Spacecraft Attitude Determination and Control*, volume 2. 2013.
- [9] Abolfazl Shirazi and Mehran Mirshams. Pyramidal reaction wheel arrangement optimization of satellite attitude control subsystem for minimizing power consumption. 15(2):190–198, 2014.
- [10] R Steven. wheel attitude control systems NAVAL POSTGRADUATE. 2013.
- [11] Maxon. EC 20 flat Ø20 mm, brushless, 5 Watt, with Hall sensors.
- [12] Faulhaber. BLDC Motors with int. Speed Controller Series 2610...B SC.
- [13] CubeSatShop. MAI-400 ADACS.
- [14] Blue Canyon Technologies. Flexcore.
- [15] CalPoly. Cubesat design specification. *The CubeSat Program, California Polytechnic State . . . , 8651(June 2004):22*, 2009.
- [16] Isaac Nason, Jordi Puig-Suari, and Robert Twiggs. Development of a family of picosatellite deployers based on the CubeSat standard. *IEEE Aerospace Conference Proceedings*, 1:457–464, 2002.

- [17] J. Puig-Suari, C. Turner, and W. Ahlgren. Development of the standard CubeSat deployer and a CubeSat class\nPicoSatellite. *2001 IEEE Aerospace Conference Proceedings (Cat. No.01TH8542)*, 1:347–353, 2001.
- [18] Thien Nguyen. Mission Design and Specification for a Space Based Aircraft Monitoring System. 2014.
- [19] Michael Swartwout. Secondary payloads in 2014: Assessing the numbers. *IEEE Aerospace Conference Proceedings*, pages 1–12, 2014.
- [20] Michael Swartwout. CubeSat Database, 2017.
- [21] Kirk Woellert, Pascale Ehrenfreund, Antonio J. Ricco, and Henry Hertzfeld. Cubesats: Cost-effective science and technology platforms for emerging and developing nations. *Advances in Space Research*, 47(4):663–684, 2011.
- [22] Jasper Bouwmeester, Martin Langer, and Eberhard Gill. Survey on the implementation and reliability of CubeSat electrical bus interfaces. *CEAS Space Journal*, 9(2):163–173, 2017.
- [23] Ch Hajiyev and M. Bahar. Attitude Determination and Control System design of KufaSat. *International Journal of Current Engineering and Technology*, 4(4):2910–2920, 2014.
- [24] CubeSatShop. MAI-400 Reaction Wheel.
- [25] CubeSpace. CubeWheel.
- [26] Blue Canyon Technologies. MICROWHEEL (RWP015).
- [27] Blue Canyon Technologies. RWP050.
- [28] Blue Canyon Technologies. RWP100.
- [29] Astrofein. Reaction Wheels.
- [30] J Straub. Cubesats: A low-cost, very high-return space technology. *Proceedings of the 2012 Reinventing Space*, 2012.
- [31] Rocket Lab USA. Space Is Open For Business, Online, 2015.
- [32] Junquan Li, Mark Post, Thomas Wright, and Regina Lee. Design of Attitude Control Systems for. *Hindawi*, 2013:1–4, 2013.
- [33] University of Sydney. CubeSat Design Overview Report of i-INSPIRE II CubeSat. pages 1–40.
- [34] Ricardo Gomes. Development of a reliable and low cost miniaturized Reaction Wheel System for CubeSat applications. 2016.
- [35] Sheen S. Levine and Michael J. Prietula. Open Collaboration for Innovation: Principles and Performance. *Organization Science*, 25(5):1414–1433, 2014.

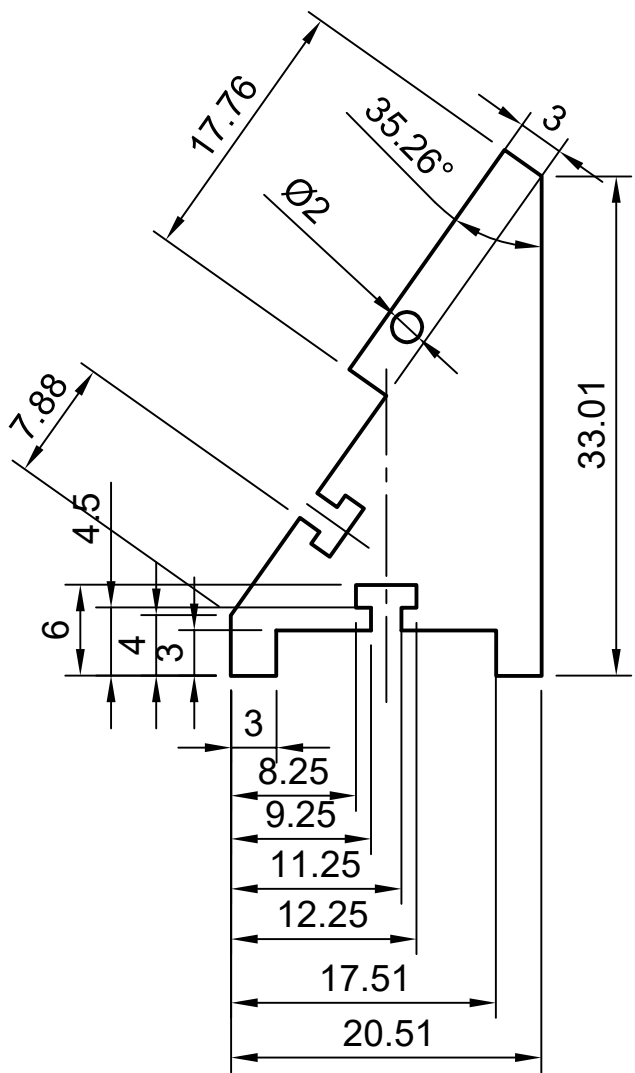
- [36] Artur Scholz and Jer Nan Juang. Toward open source CubeSat design. *Acta Astronautica*, 115(June 2003):384–392, 2015.
- [37] James Bultitude, Ben Southwell, Tim Broadbent, Yiwei Han, Li Qiao, Joon Wayn Cheong, and Barnaby Osborne. Attitude Determination and Control System Implementation for the EC0 (QB50 Project) at UNSW. 2016.
- [38] Nasa Goddard, Space Flight, Reid G Reynolds, and Millennium Space Systems. Maximum Torque and Momentum Envelopes for Reaction-Wheel Arrays. 33(5), 2010.
- [39] Emfforce O P S Manual. Reaction Wheel Design. pages 1–11, 2003.
- [40] Peter Bugryniec. CubeSat : The Need for More Power to Realise Telecommunications Overview of CubeSats Aims & Objectives. (June):1–10, 2016.

RWS Mechanical Drawings

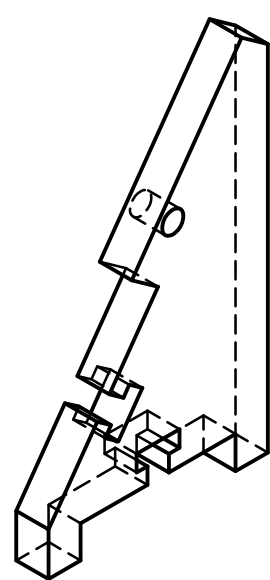
This appendix contains mechanical drawings for components in the RWS design. All units are in mm unless marked otherwise.



TOP VIEW

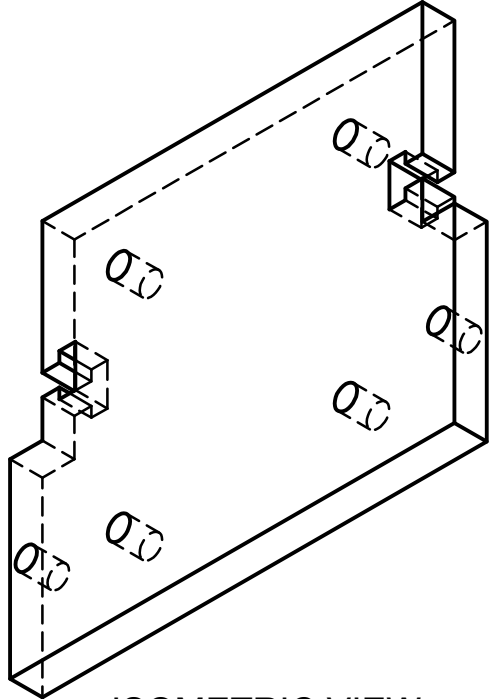


FRONT VIEW

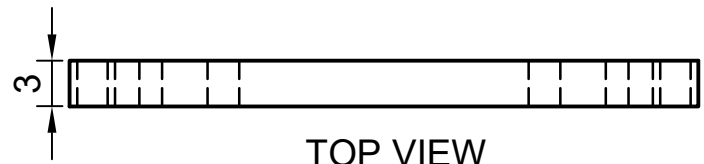


ISOMETRIC VIEW

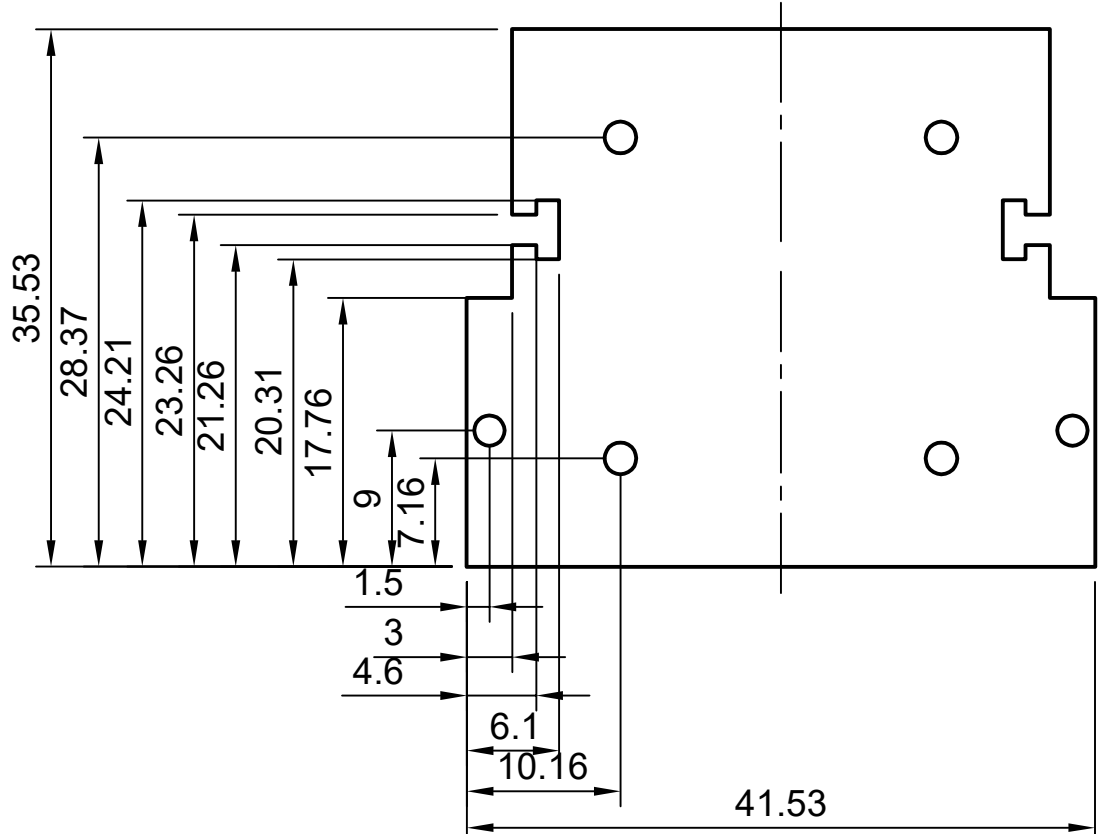
Dept.	Technical reference	Created by Mark Yeo	Approved by
		2018-05-25	
	Document type	Document status	
	Title MotAssemblyV2	DWG No.	
	Rev.	Date of issue	Sheet 1/1



ISOMETRIC VIEW

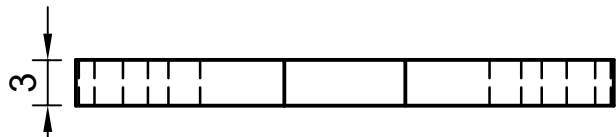


TOP VIEW



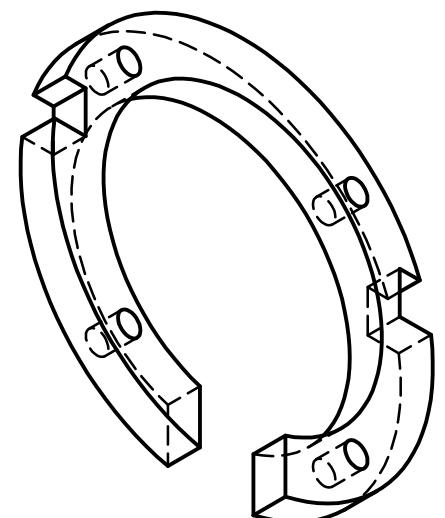
FRONT VIEW

Dept.	Technical reference	Created by Mark Yeo 2018-05-25	Approved by
Document type		Document status	
Title MotAssemblyV2		DWG No.	
Rev.	Date of issue	Sheet	1/1

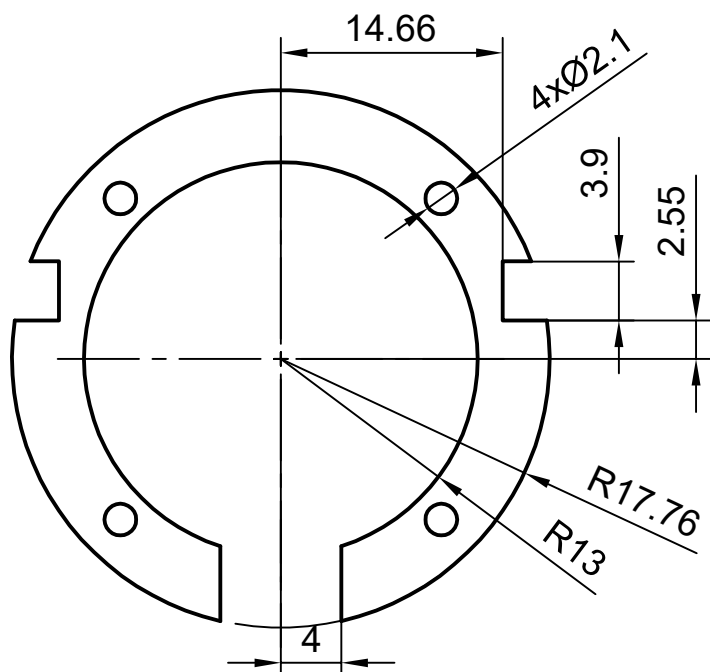


3

TOP VIEW

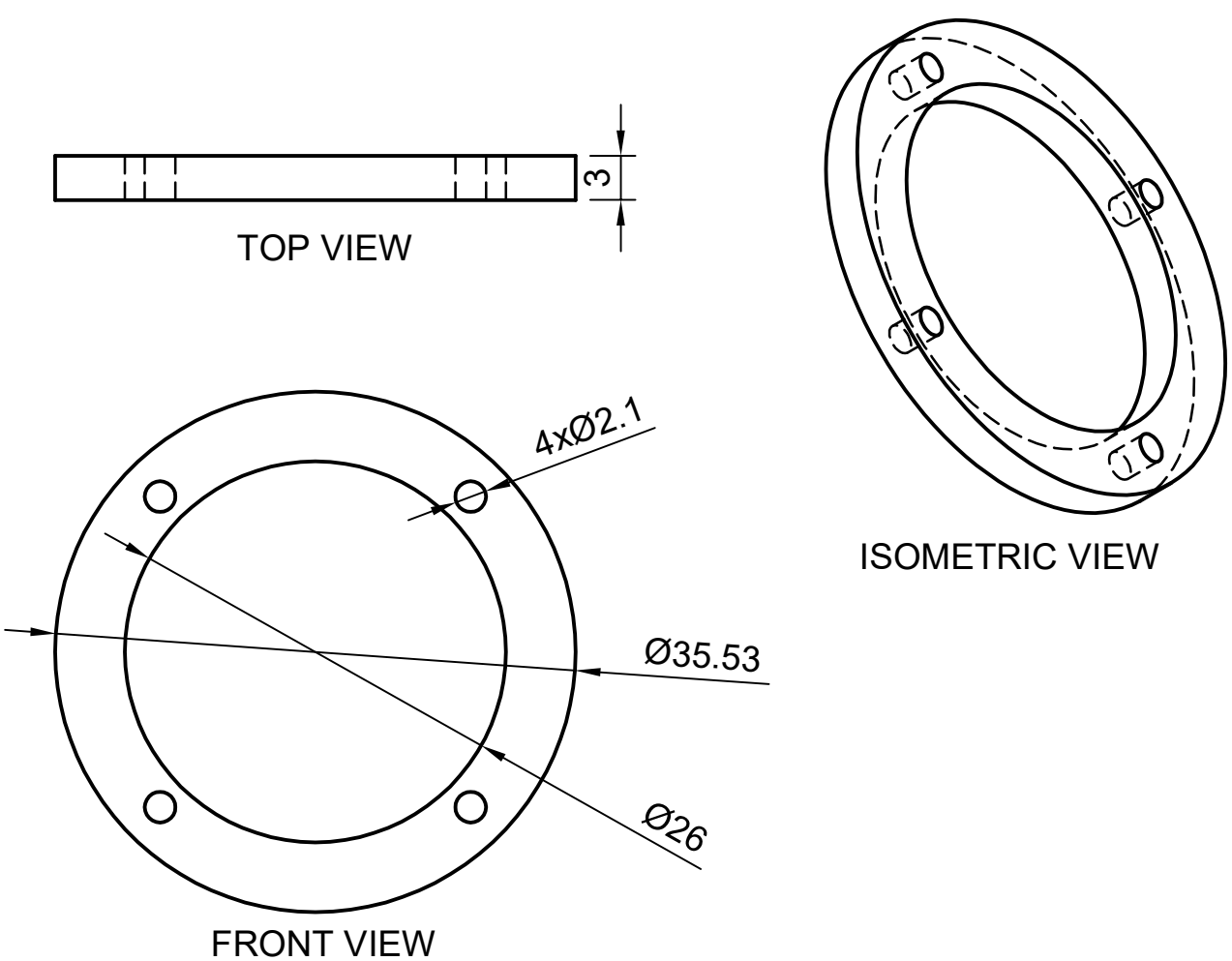


ISOMETRIC VIEW

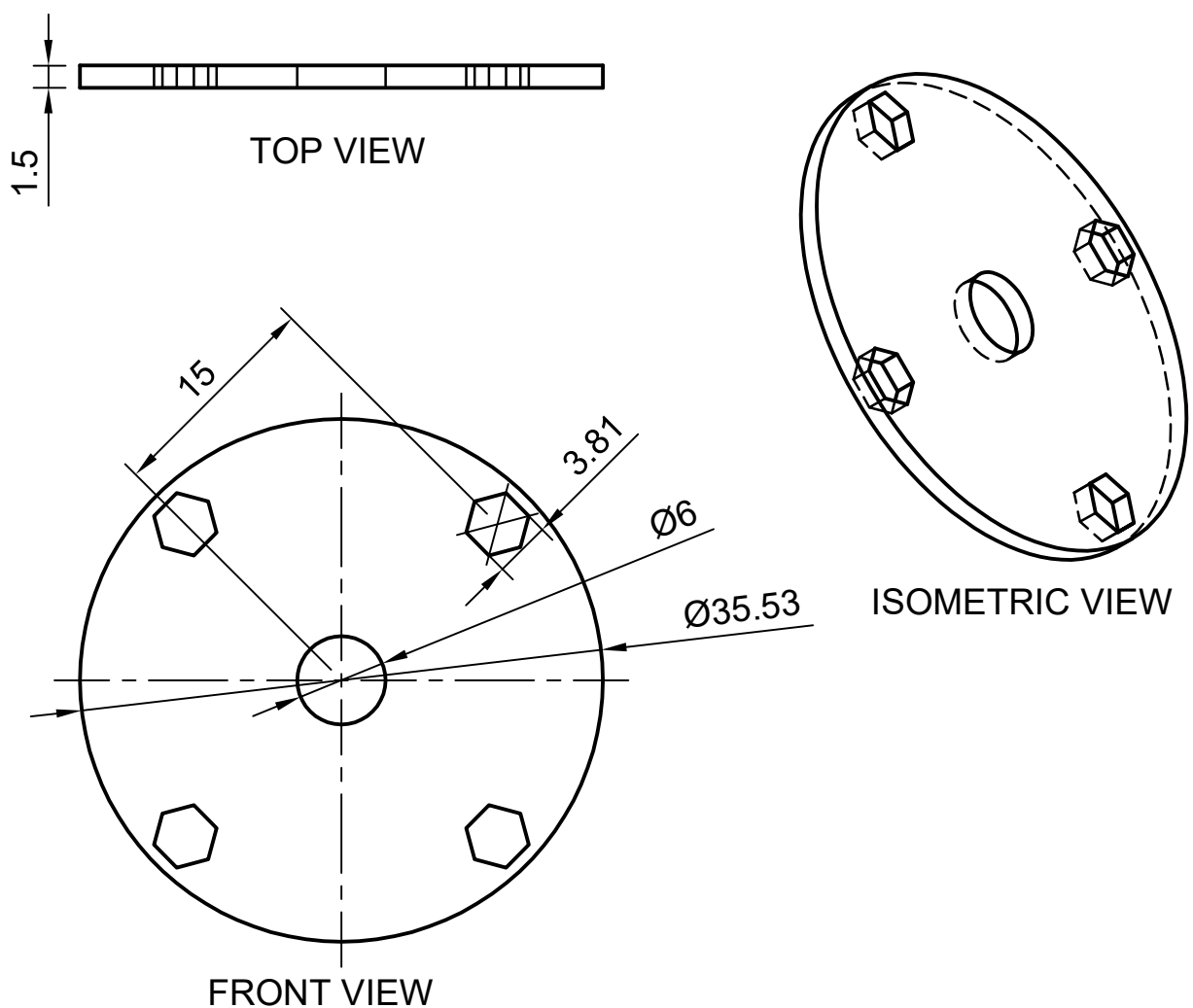


FRONT VIEW

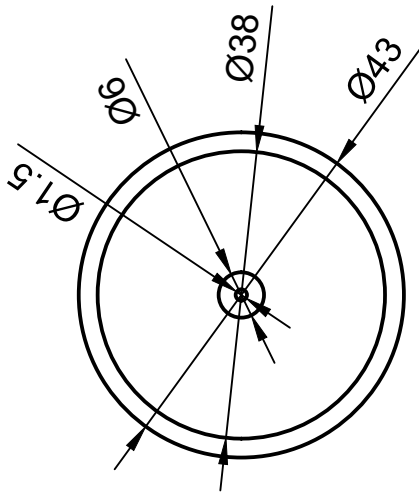
Dept.	Technical reference	Created by Mark Yeo 2018-05-25	Approved by
		Document type	Document status
Title MotAssemblyV2		DWG No.	
		Rev.	Date of issue
		Sheet 1/1	



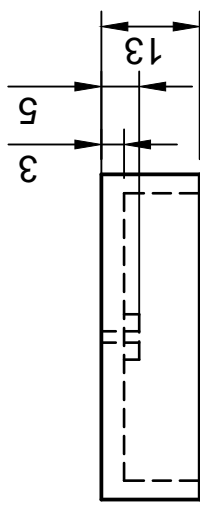
Dept.	Technical reference	Created by Mark Yeo 2018-05-25	Approved by
	Document type	Document status	
	Title MotAssemblyV2	DWG No.	
	Rev.	Date of issue	Sheet 1/1



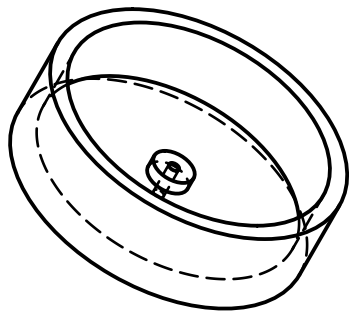
Dept.	Technical reference	Created by Mark Yeo 2018-05-25	Approved by
		Document type	Document status
Title MotAssemblyV2		DWG No.	
		Rev.	Date of issue
		Sheet 1/1	



BOTTOM VIEW

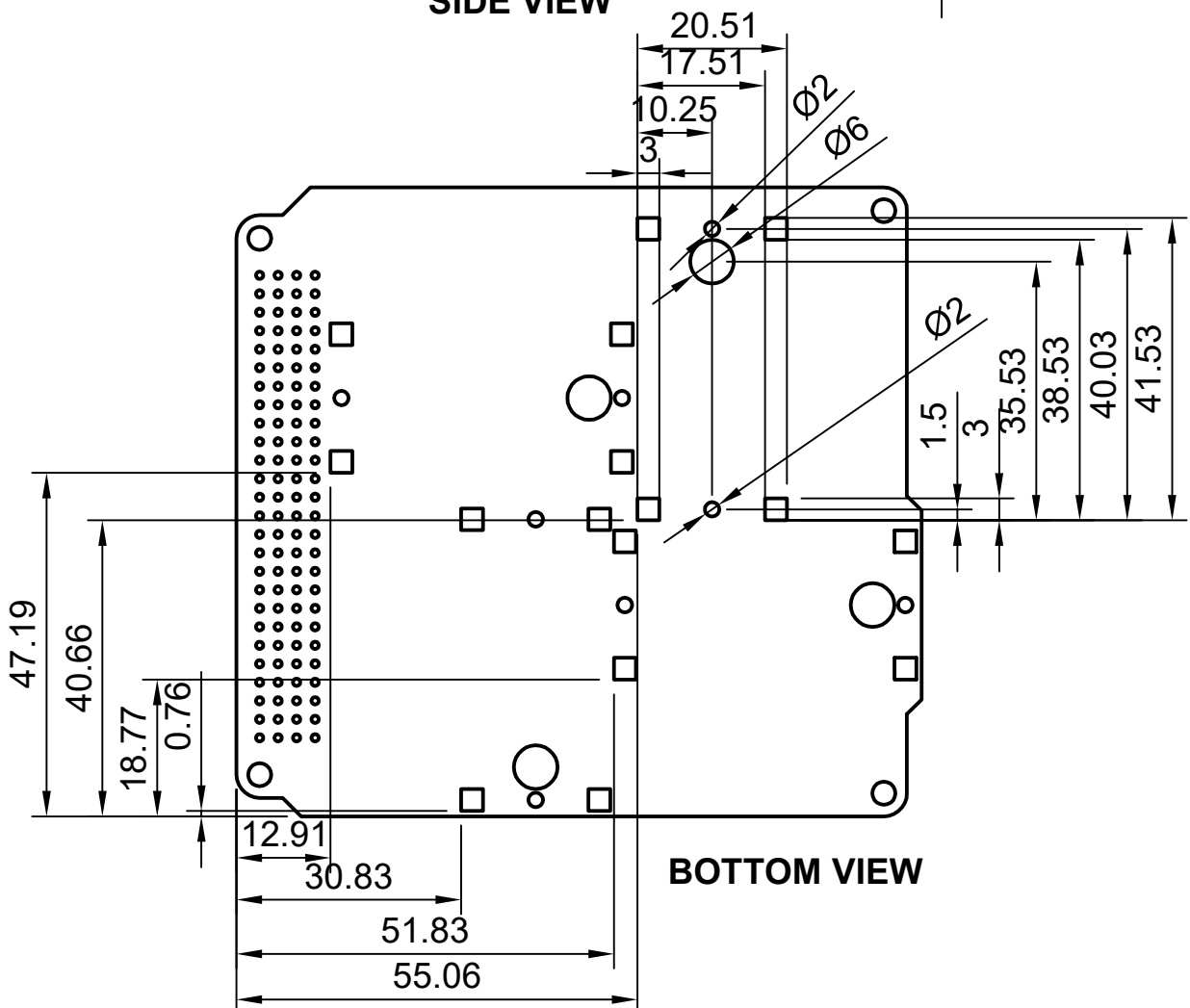
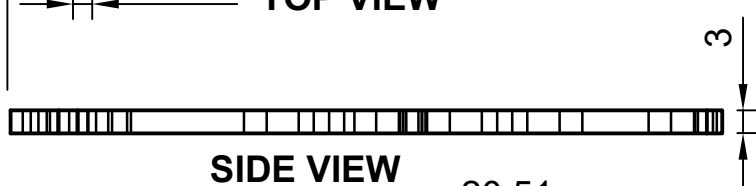
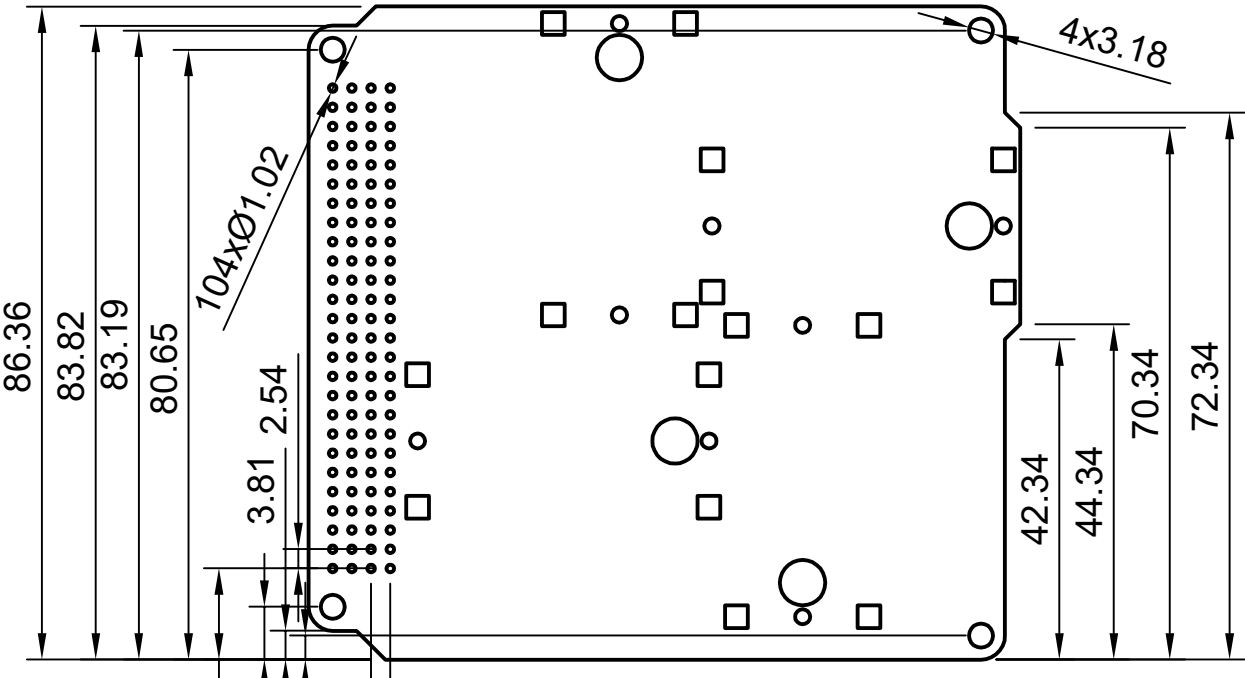


FRONT VIEW



ISOMETRIC VIEW

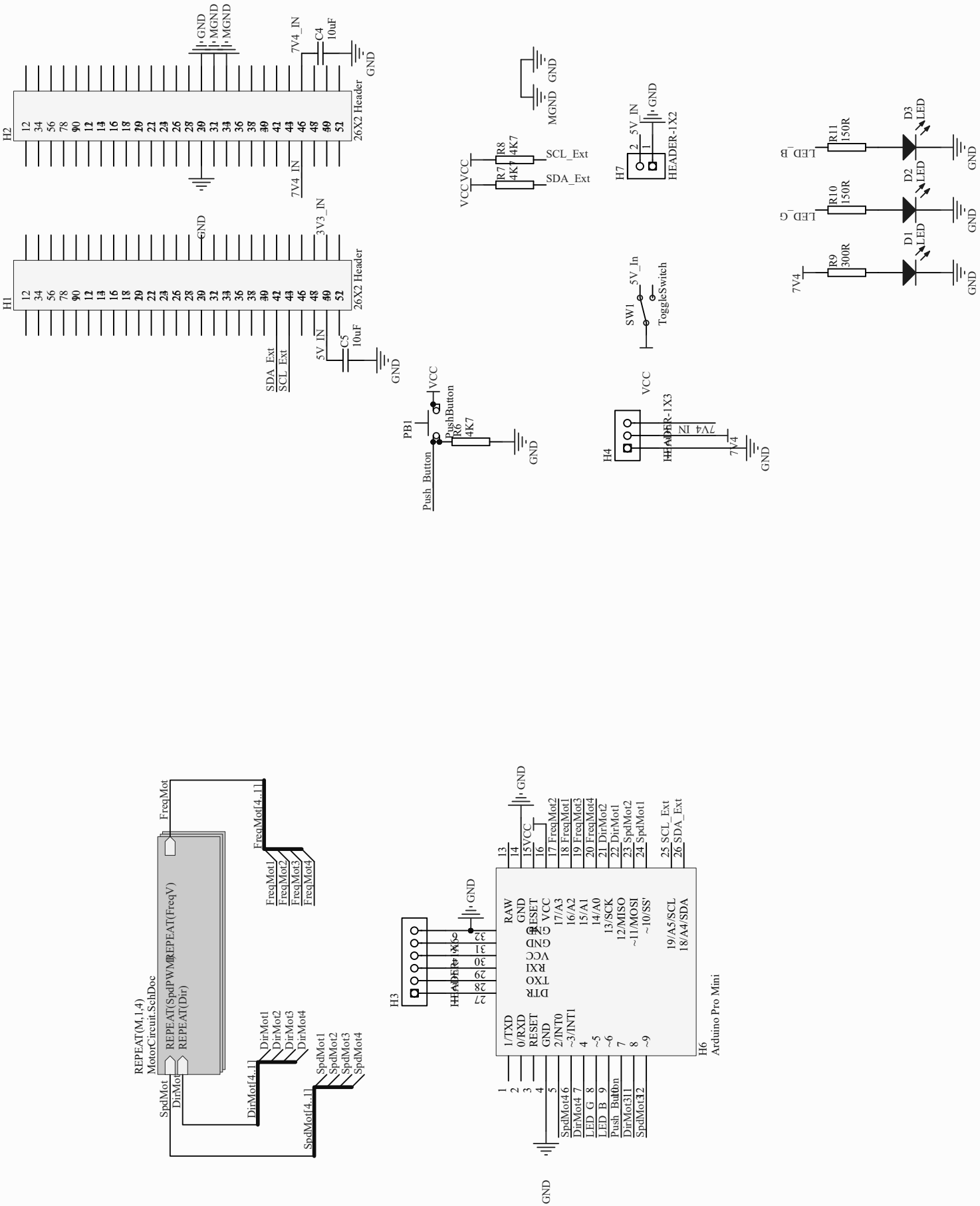
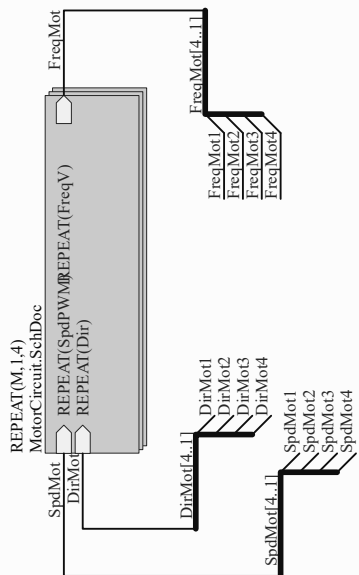
Dept.	Technical reference	Created by Mark Yeo	Approved by
All Dimensions in mm	Document type	2018-03-12	Document status
	Title	Wheel	DWG No.
	Rev.	Date of issue	Sheet 1/1

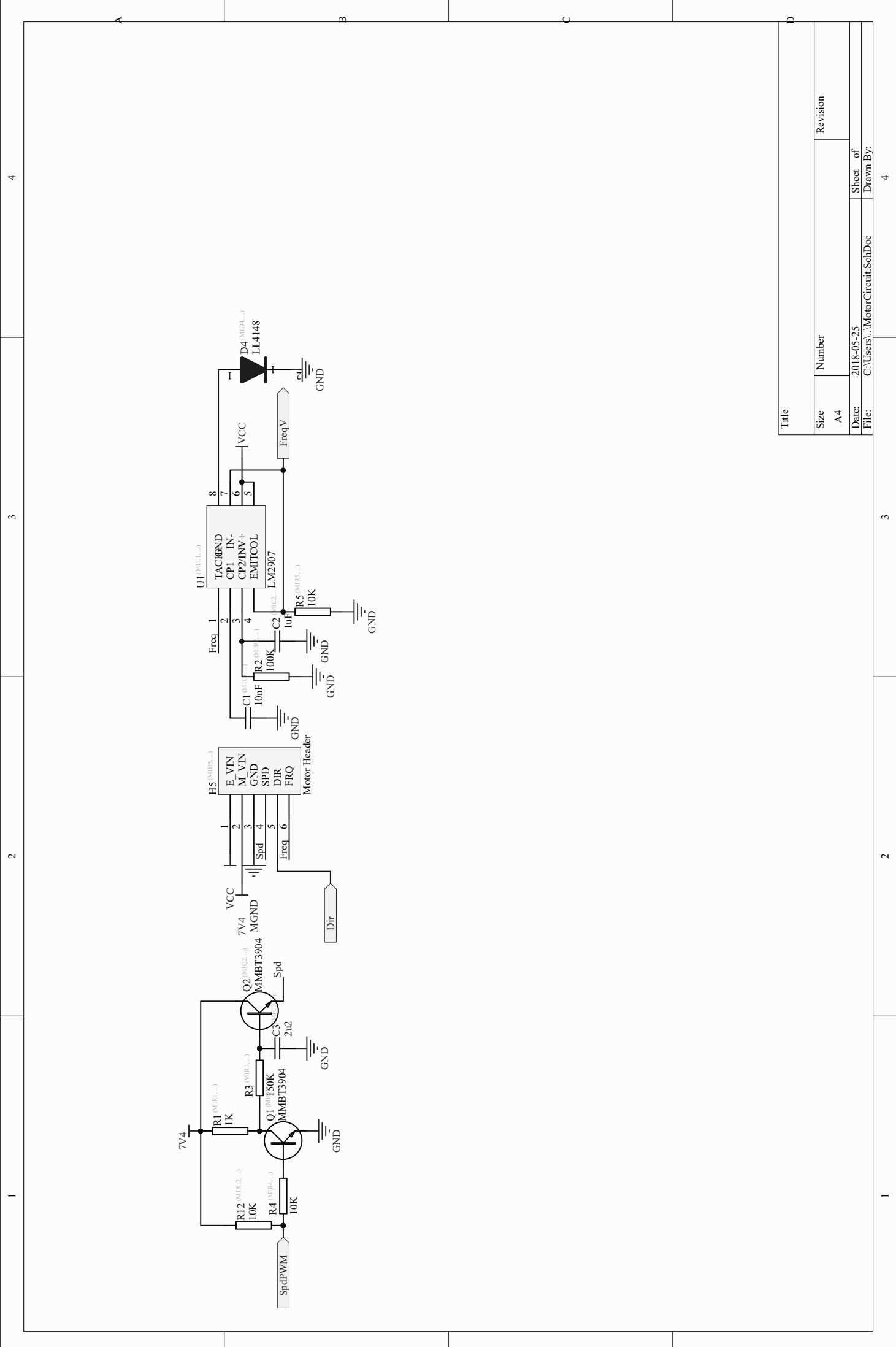


MOUNTING PLATE

RWS Electrical Schematics

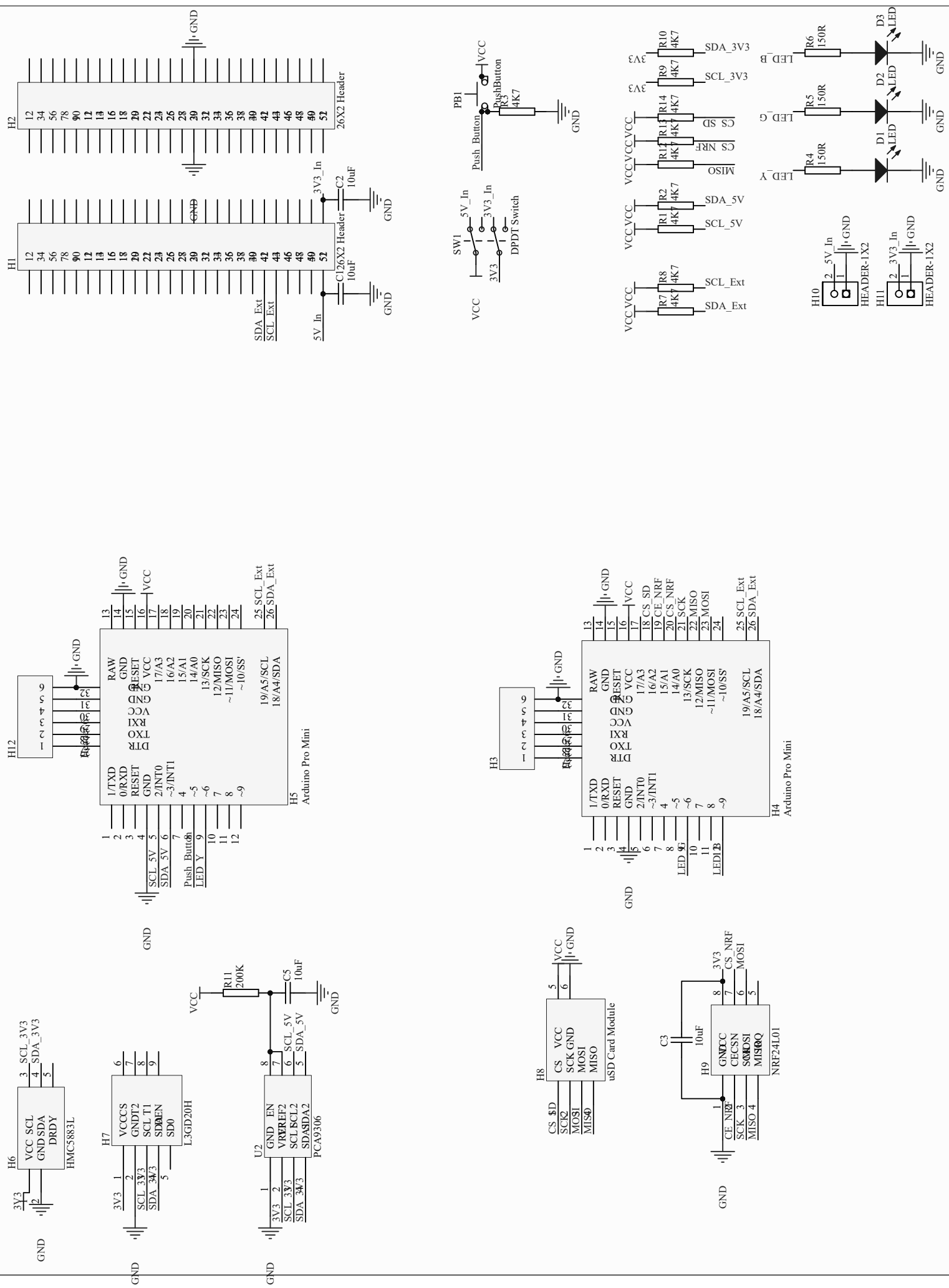
This appendix contains electrical schematics for RWS electronics.

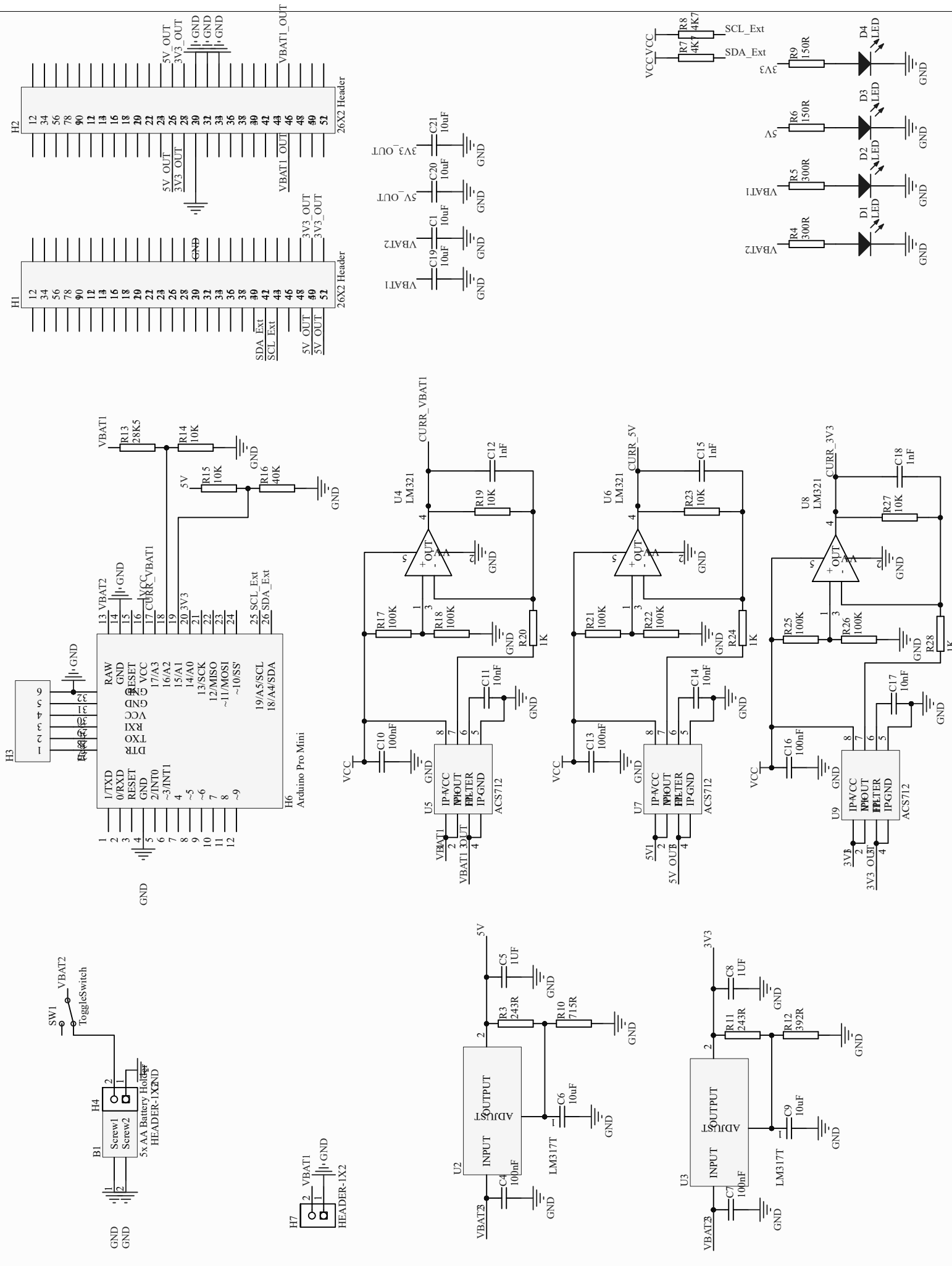




Support Hardware Electrical Schematics

This appendix contains electrical schematics for the ADCS/Comms and Power/OBC boards.





Complete Test Results

This appendix contains the complete results of the RWS tests.

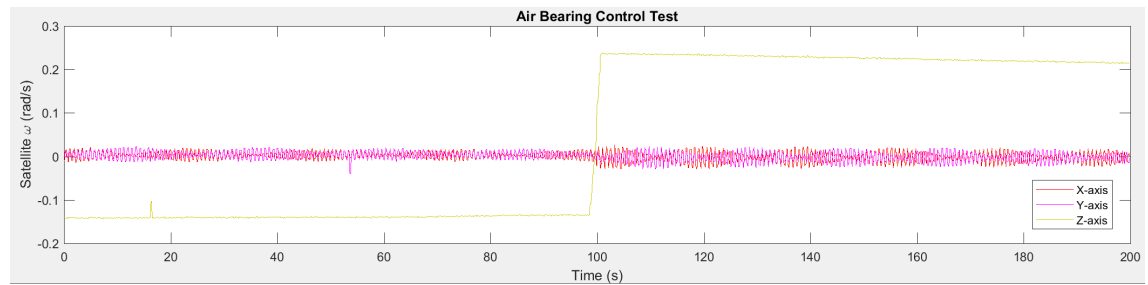


Figure D.1: Air Bearing Natural Spin Decay.
Note that spin was manually reversed at 100s

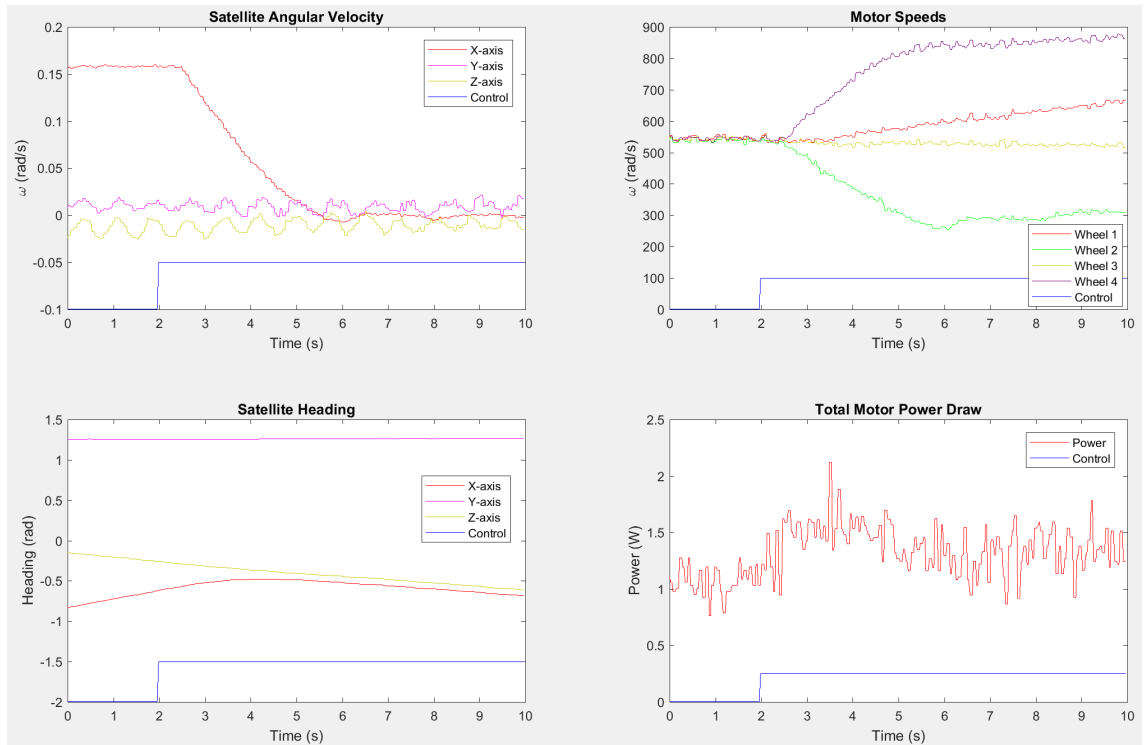


Figure D.2: Detumble Performance around X+ Axis

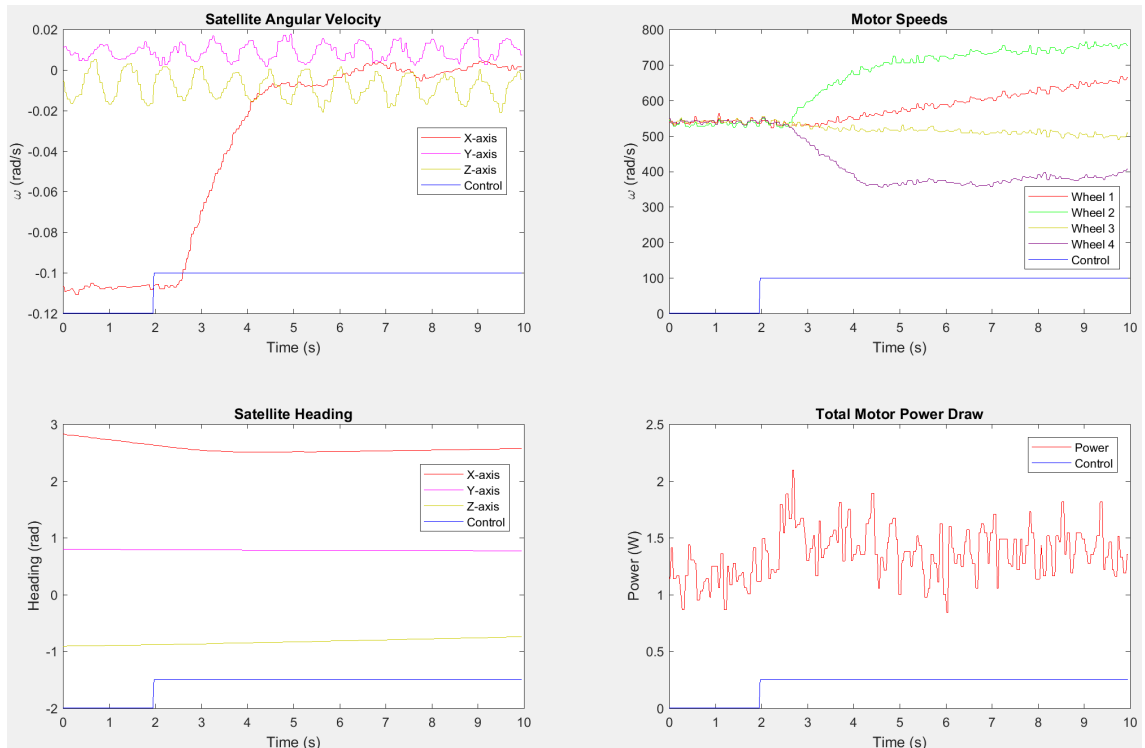


Figure D.3: Detumble Performance around X- Axis

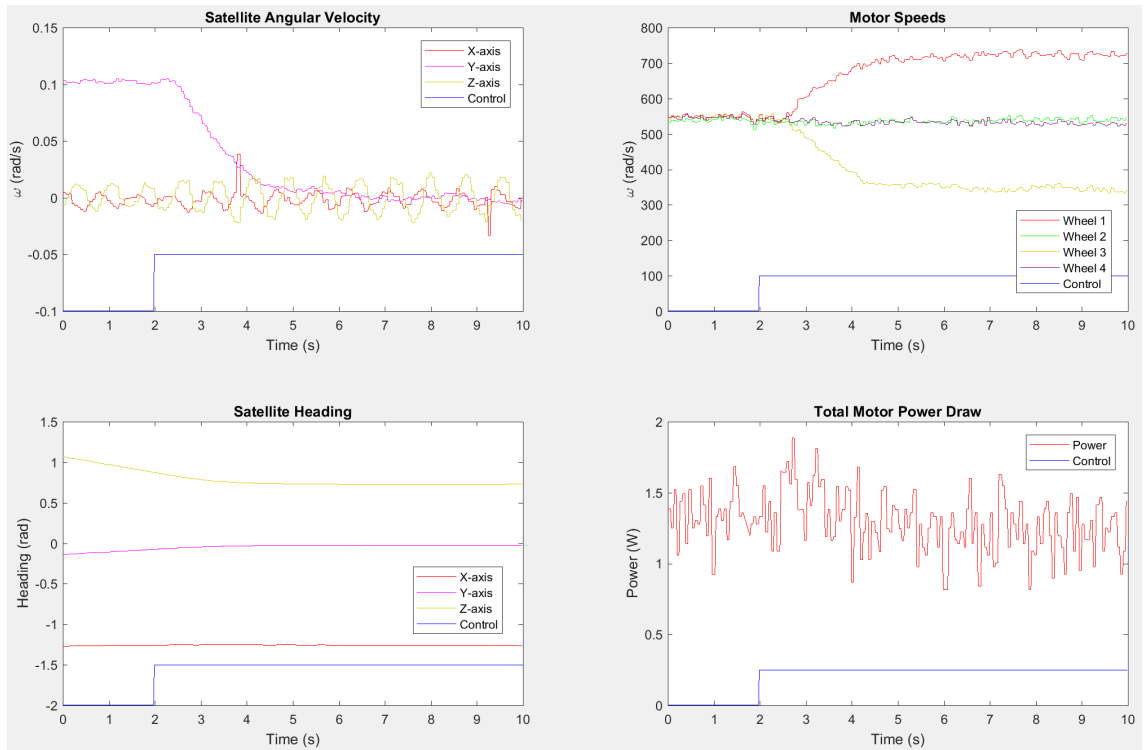


Figure D.4: Detumble Performance around Y+ Axis

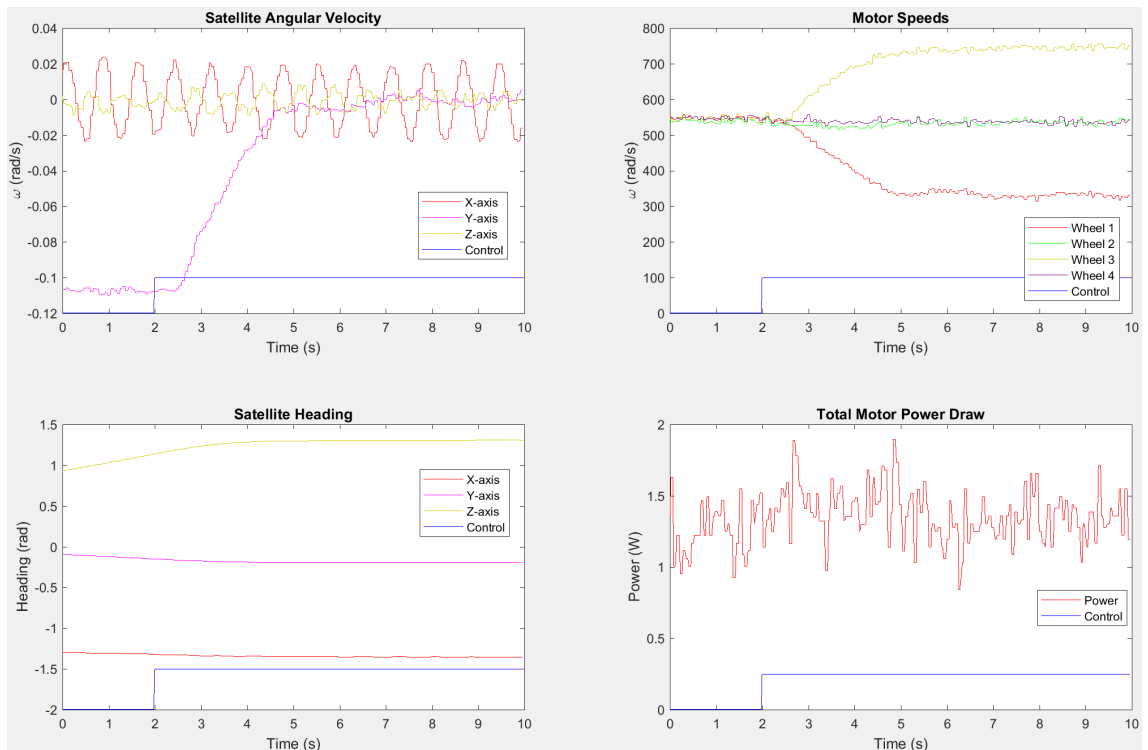


Figure D.5: Detumble Performance around Y- Axis

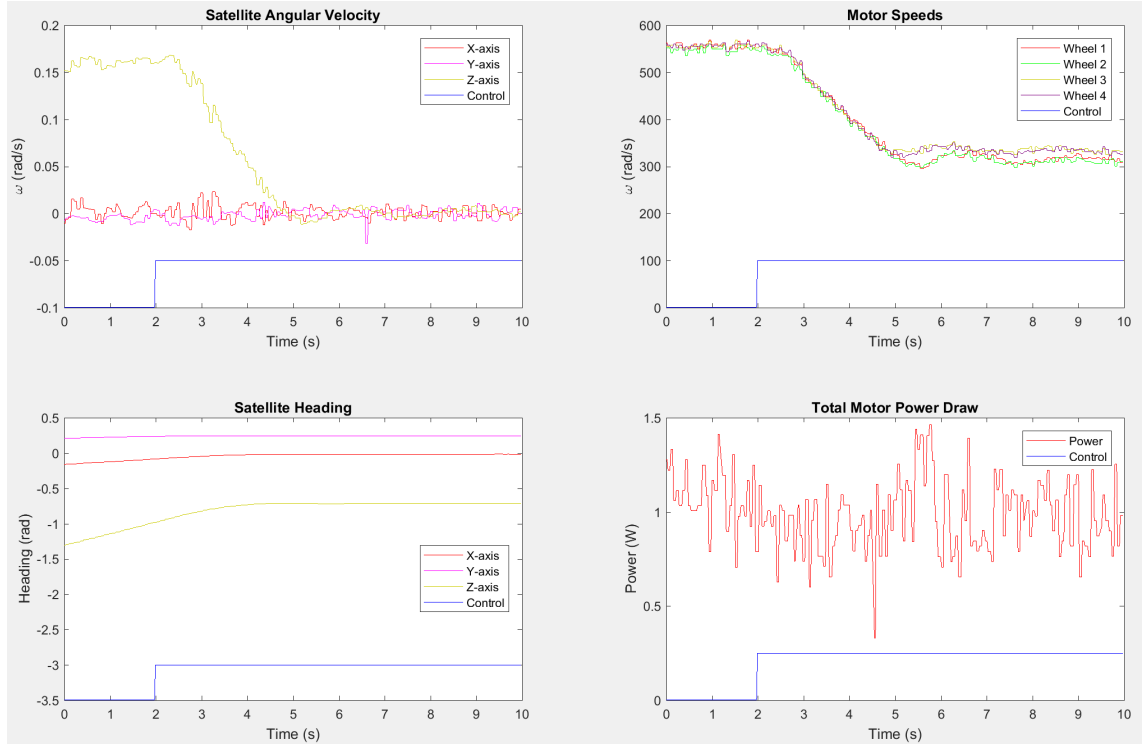


Figure D.6: Detumble Performance around Z+ Axis

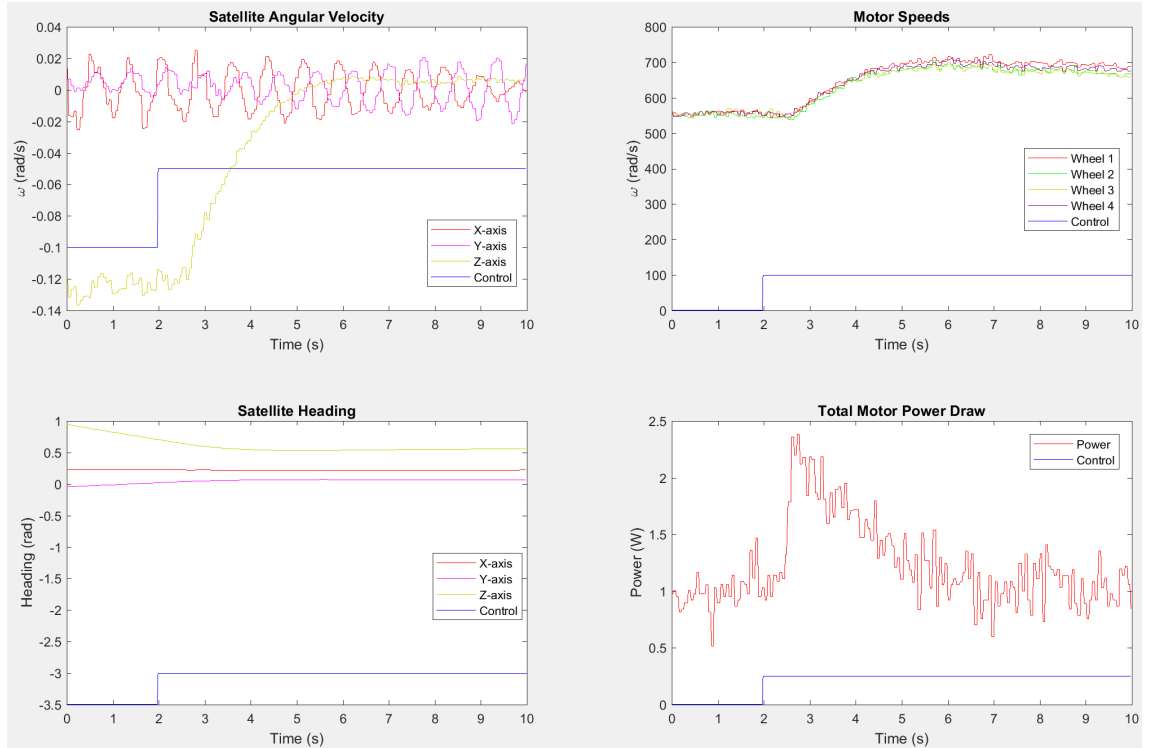


Figure D.7: Detumble Performance around Z- Axis

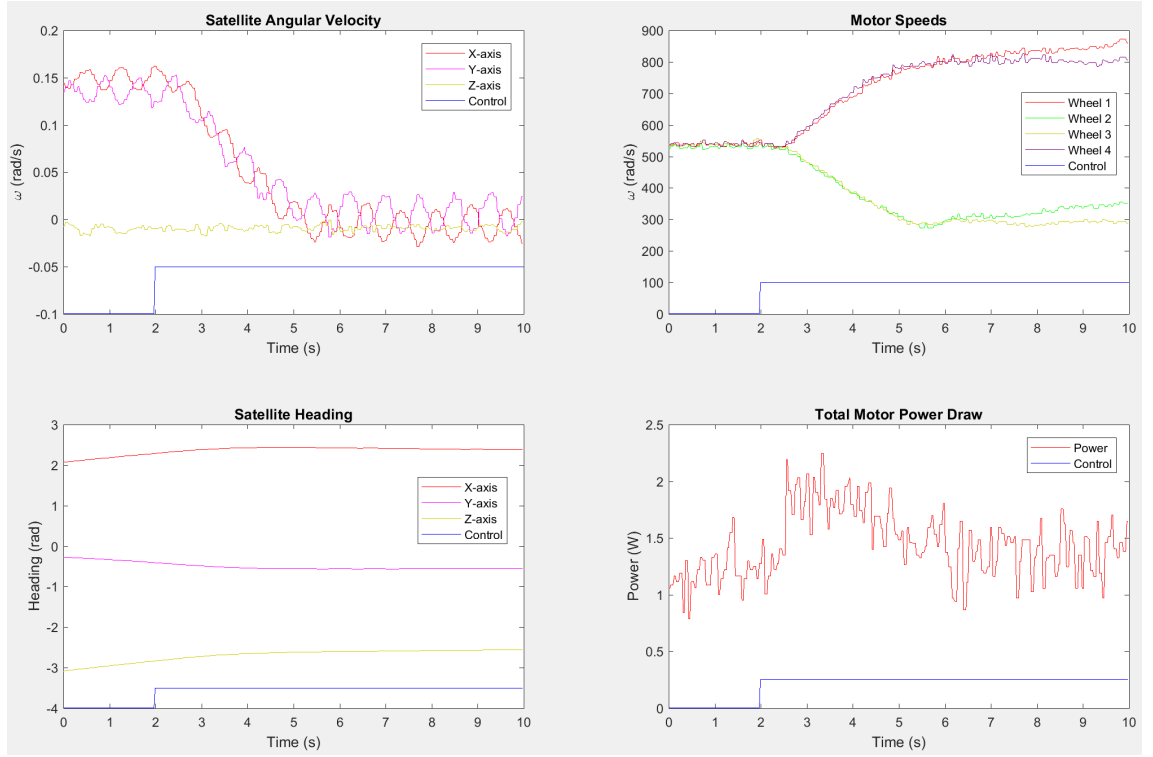


Figure D.8: Detumble Performance around X+Y+ Axis

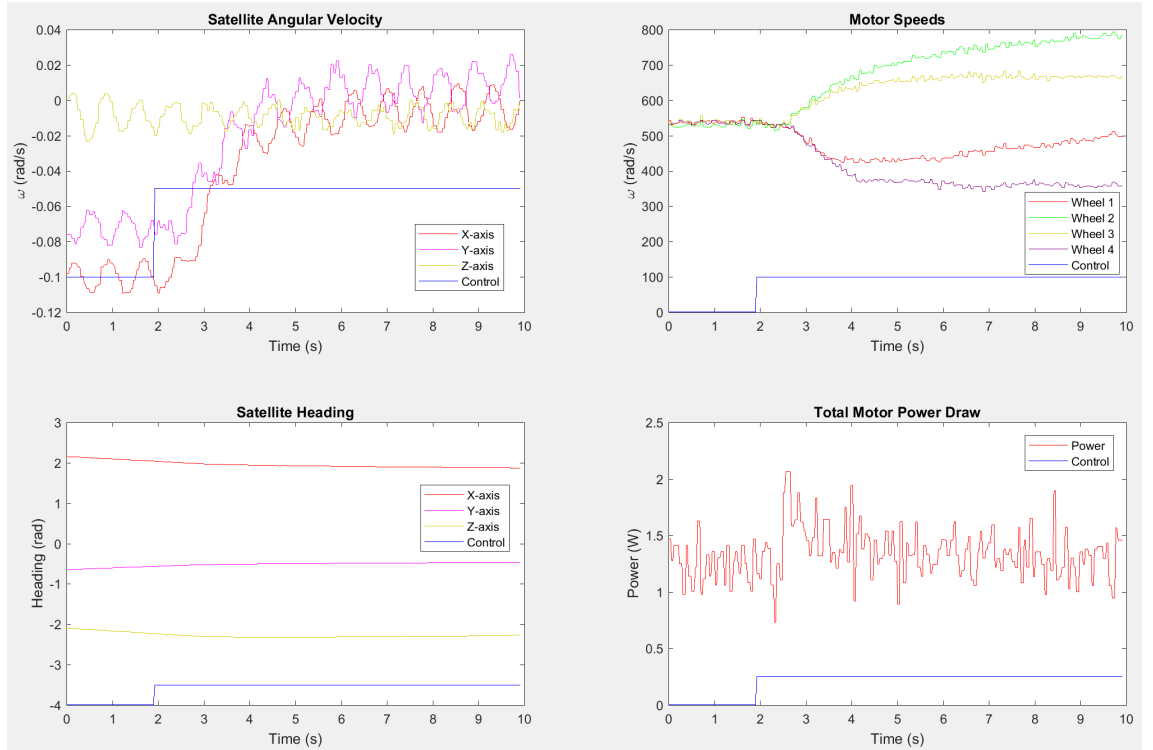


Figure D.9: Detumble Performance around X-Y- Axis

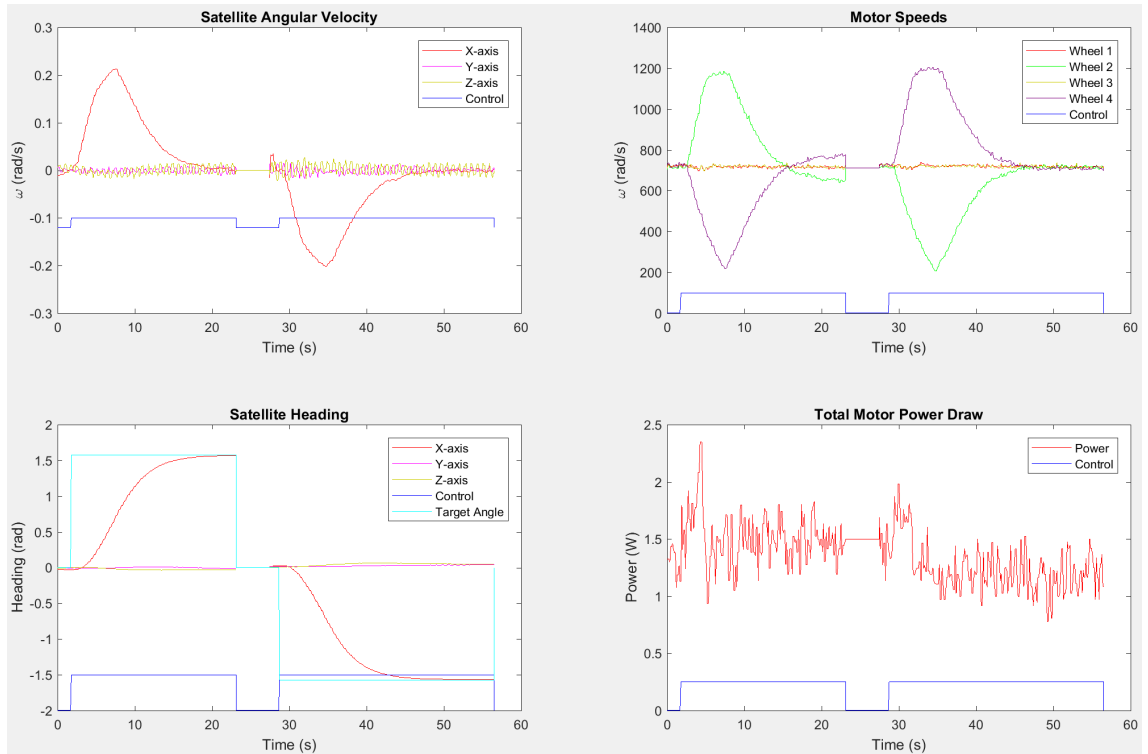


Figure D.10: Pointing Performance around X Axis

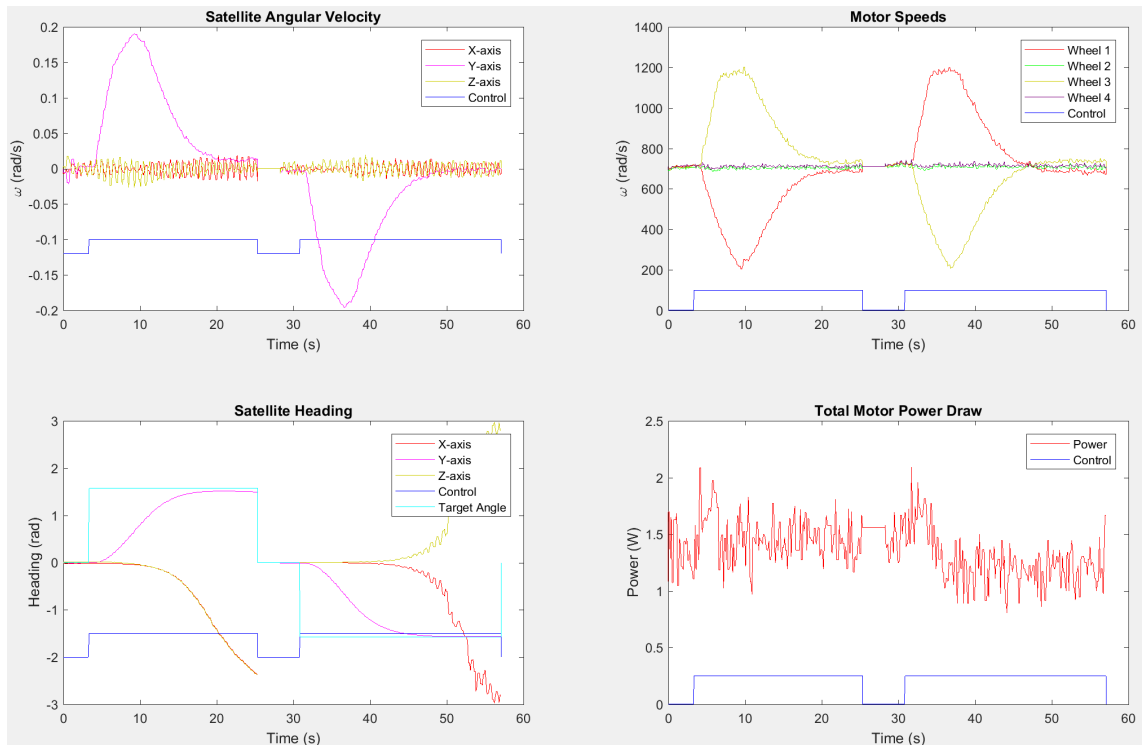


Figure D.11: Pointing Performance around Y Axis

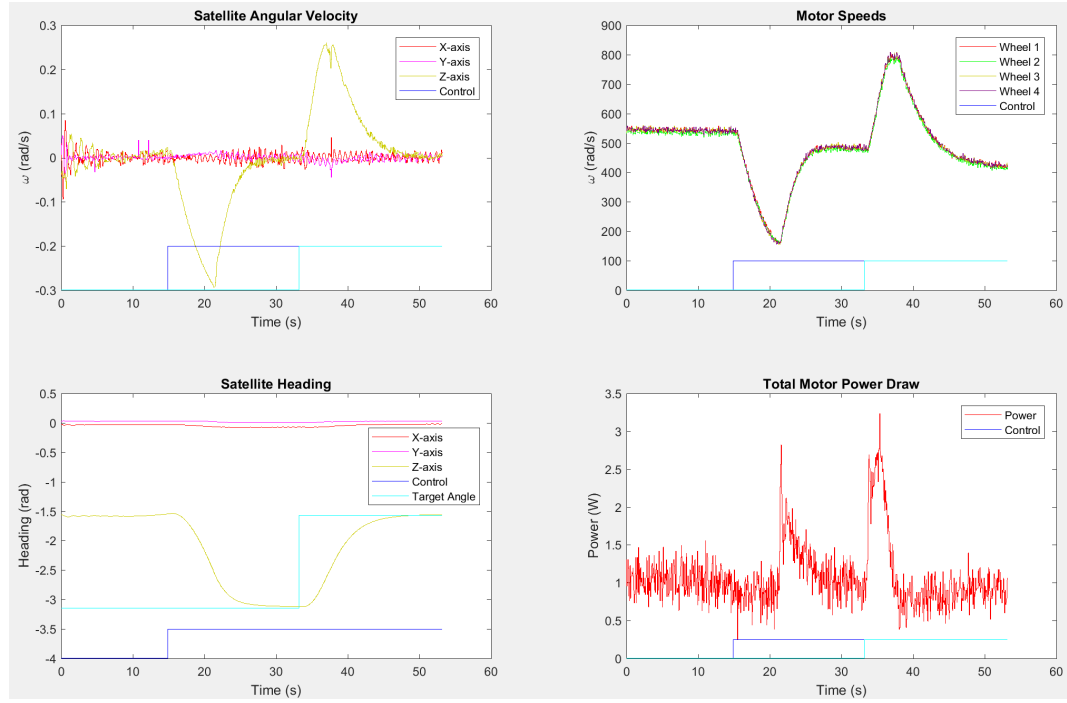


Figure D.12: Pointing Performance around Z Axis.
Note that the target angle of $+180^\circ$ is shown as -180° for ease of reading.

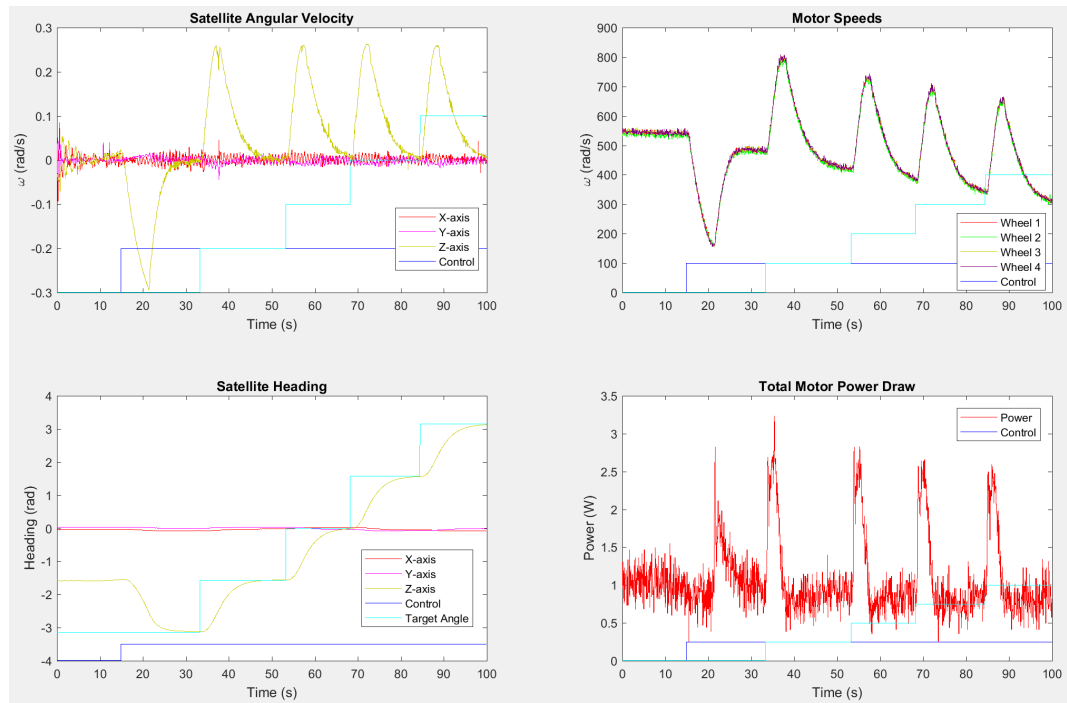


Figure D.13: Pointing Performance around Z Axis

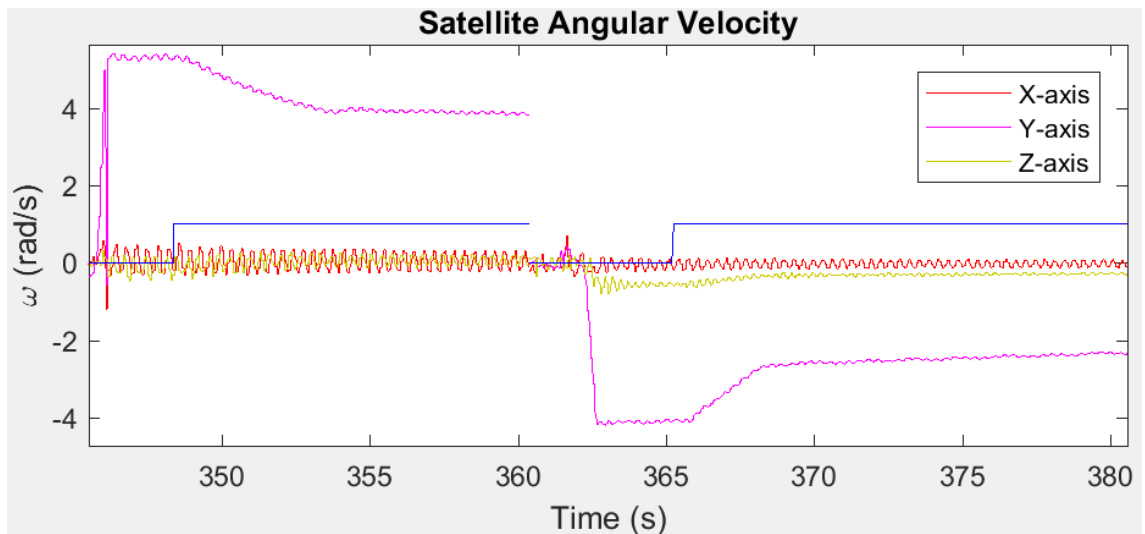


Figure D.14: Momentum Capacity around Y Axis

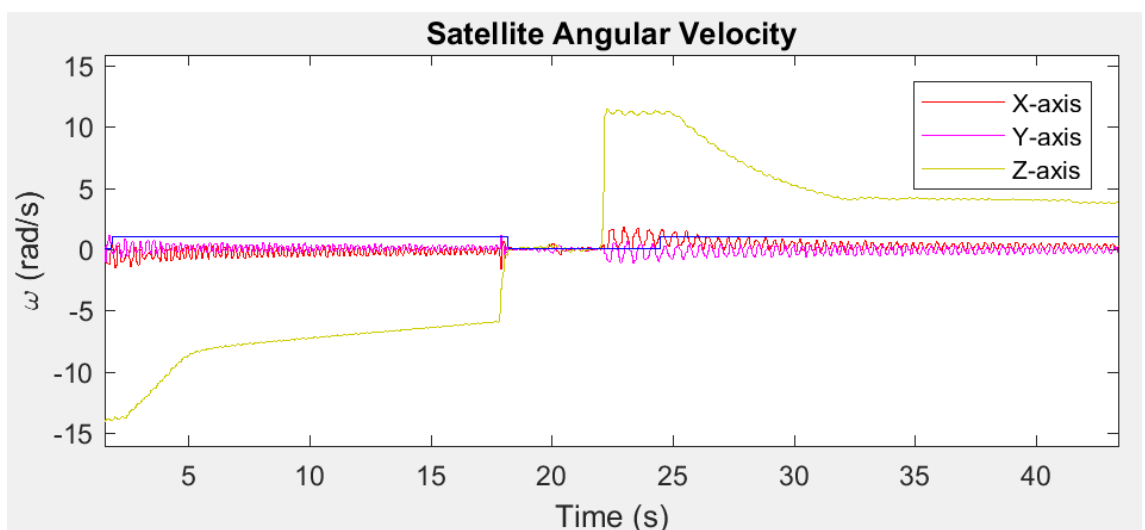


Figure D.15: Momentum Capacity around Z Axis

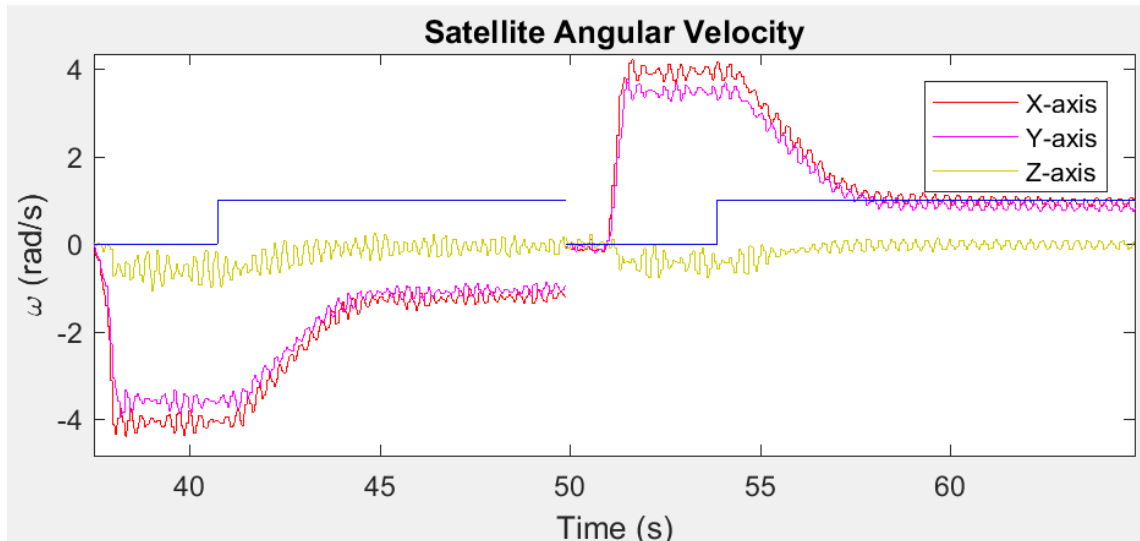


Figure D.16: Momentum Capacity around XY Axis

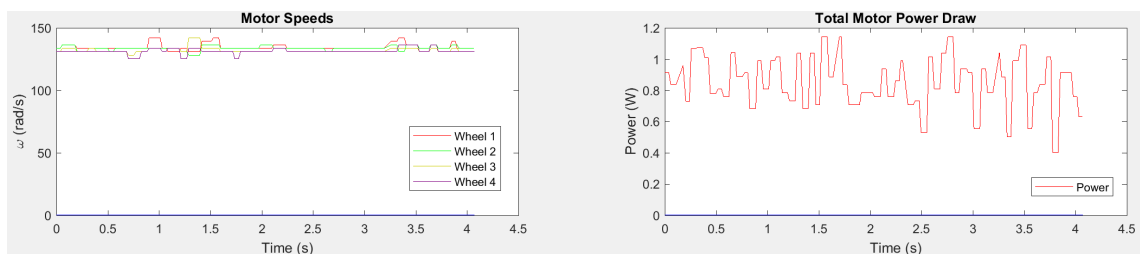


Figure D.17: Motor Power Draw at Zero Speed

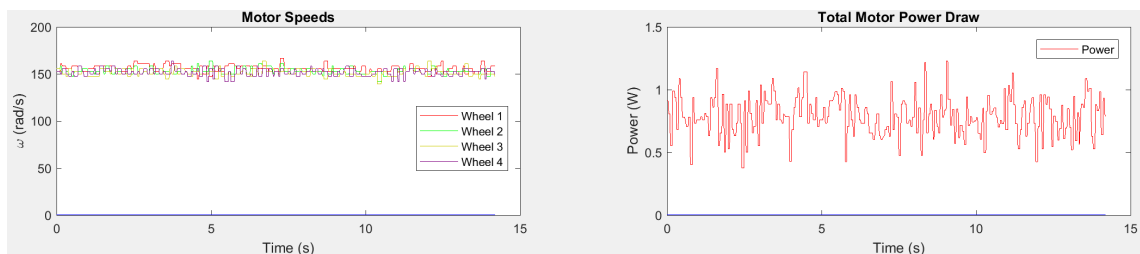


Figure D.18: Motor Power Draw at Minimum Linear Speed

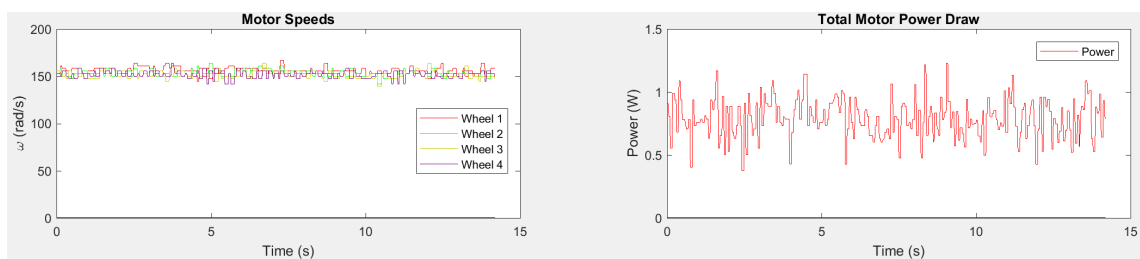


Figure D.19: Motor Power Draw at Full Speed

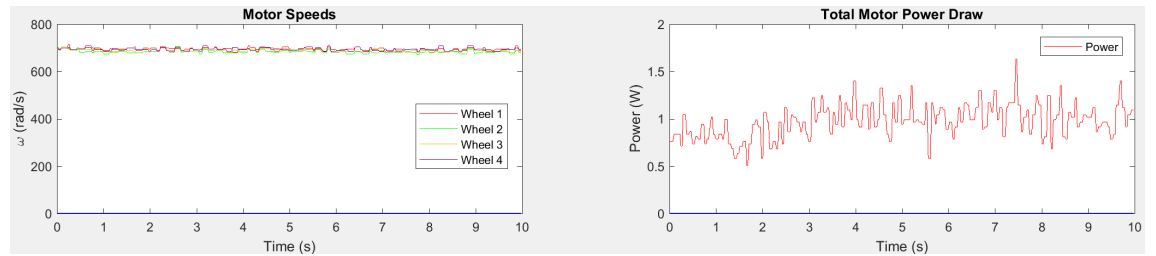


Figure D.20: Motor Power Draw at Medium Speed

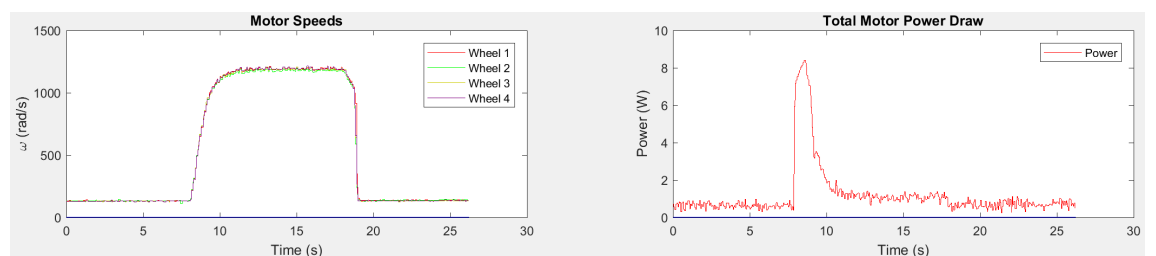


Figure D.21: Motor Power Draw from Zero to Full Speed with Maximum Acceleration

Other Datasheets

This appendix contains datasheets for the RWS motors and the air bearing used in testing.

Brushless Flat DC-Micromotors

with integrated Speed Controller

3,12 mNm

1,6 W

2610 ... B SC

Values at 22°C and nominal voltage	2610 T	006 B SC	012 B SC
Power supply electronic	U_p	4 ... 18	4 ... 18
Power supply motor	U_{mot}	1,7 ... 18	1,7 ... 18
Nominal voltage for motor	U_N	6	12
No-load speed (at U_N)	n_0	6 700	6 650
Peak torque (S2 operation for max. 2s/1s)	$M_{max.}$	6	6
Torque constant	k_M	9,05	18,1
PWM switching frequency	f_{PWM}	96	96
Efficiency electronic	η	95	95
Standby current for electronic (at U_N)	I_{el}	0,02	0,02
Speed range (up to 12V / 18V)		400 ... 13 300	400 ... 10 000
Shaft bearings	ball bearings, preloaded		
Shaft load max.:			
- with shaft diameter	1,5		mm
- radial at 3 000 min ⁻¹ (3 mm from mounting flange)	4		N
- axial at 3 000 min ⁻¹ (push only)	3,5		N
- axial at standstill (push only)	17,5		N
Shaft play:			
- radial	$\leq 0,015$		µm
- axial	= 0		µm
Operating temperature range	-25 ... +80		°C
Housing material	plastic		
Mass	20,1		g

Rated values for continuous operation

Rated torque	M_N	3,25	3,12	mNm
Rated current (thermal limit)	I_N	0,53	0,29	A
Rated speed	n_N	1 600	1 300	min ⁻¹

Interface / range of functions

... SC
Configuration from Motion Manager 5.0
via USB Programming Adapter
Operating modes
Integrated speed control via PI controller and external set value specification; communication via digital Hall sensors. Can optionally be operated in voltage controller mode or fixed speed mode.
Speed range
Digital Hall = from 400 min ⁻¹
Additional functions
Integrated current limiting to protect against thermal overload. Intermittent operation (S2) with up to double the continuous current. Separate voltage supply for motor and electronics. Direction of rotation changeover through separate switching input; reading of speed signal via frequency output.

Note:

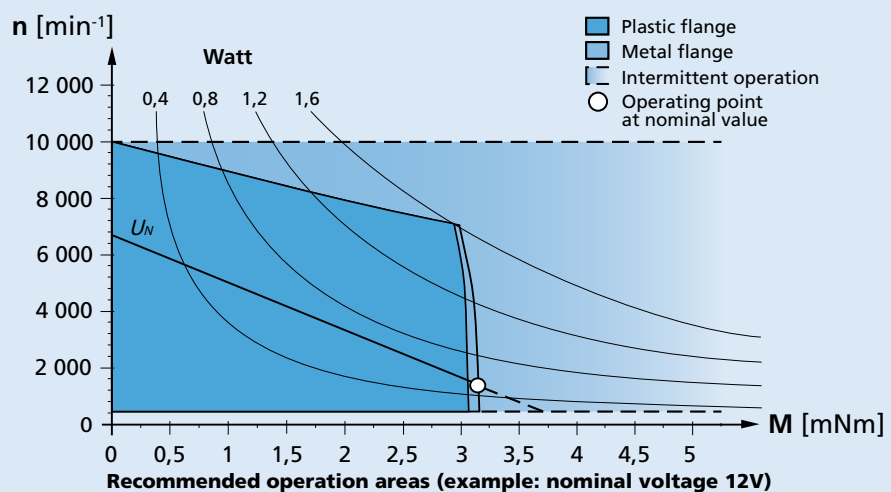
The display shows the range of possible operation points of the drives at a given ambient temperature of 22°C.

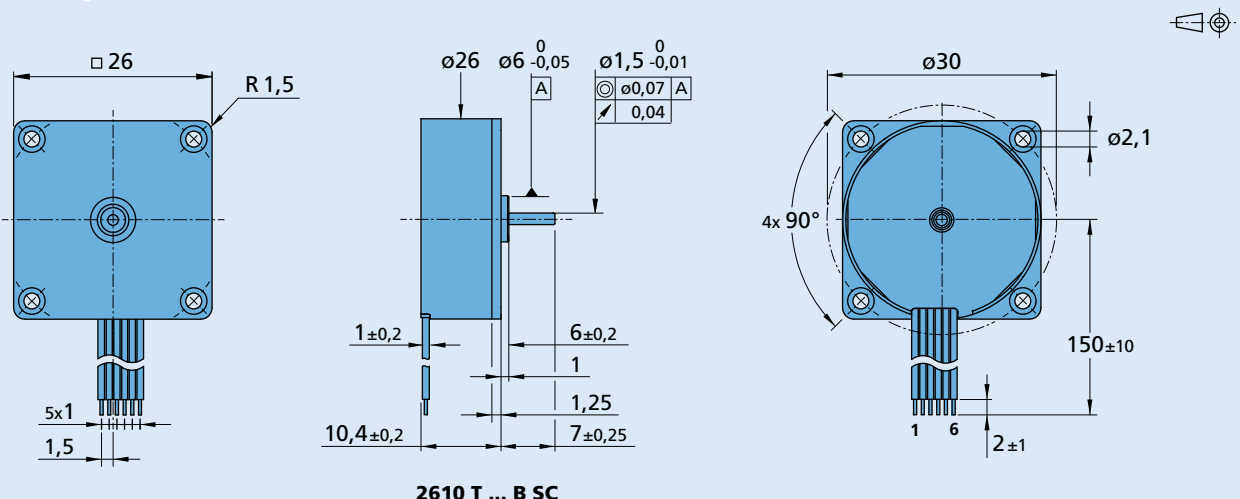
The diagram indicates the recommended speed in relation to the available torque at the output shaft.

It includes the assembly on a plastic- as well as on a metal flange (assembly method: IM B 5).

The nominal voltage linear slope describes the maximal achievable operating points at nominal voltage.

Any points of operation above this linear slope will require a supply voltage $U_{mot} > U_N$.



Dimensional drawing

Option, cable and connection information

Example product designation: **2610T012BSC-4257**

Option	Type	Description	Connection			
			Name	Function	Inputs-outputs	Description
4257	Connector	AWG 28 / PVC ribbon cable with connector Picoblade 	1	<i>UP</i>	power supply electronic	4 ... 18 V DC
			2	<i>Umot</i>	power supply motor	1,7 ... 18 V DC
			3	GND	ground	
			4	<i>Un soll</i>	input voltage input resistance set speed value	<i>Uin</i> = 0 ... 10 V > 10 V ... <i>Up</i> » set speed value not defined <i>Rin</i> ≥ 8,9 kΩ per 1 V, 1.000 min⁻¹ <i>Uin</i> < 0,15 V » motor stops <i>Uin</i> > 0,3 V » motor starts
			5	DIR	direction of rotation input resistance	to ground or level < 0,5 V » counterclockwise open or level > 3 V » clockwise <i>Rin</i> ≥ 10 kΩ
			6	FG	frequency output	max. <i>Up</i> ; <i>Imax</i> = 15 mA; open collector with 22 kΩ pull-up resistor 6 lines per revolution
			Standard cable PVC ribbon cable 6 x AWG 28, 1 mm			
			Note: For details on the connection assignment, see device manual for the SCS.			

Product combination

Precision Gearheads / Lead Screws	Encoders	Drive Electronics	Cables / Accessories
		Integrated	To view our large range of accessory parts, please refer to the "Accessories" chapter.

